







ORIGINAL RESEARCH

# Carfilzomib Treatment Causes Molecular and Functional Alterations of Human Induced Pluripotent Stem Cell–Derived Cardiomyocytes

Parvin Forghani , PhD; Aysha Rashid, BS; Fangxu Sun, PhD; Rui Liu , BS; Dong Li , PhD; Megan R. Lee, BS; Hyun Hwang , BS; Joshua T. Maxwell , PhD; Anant Mandawat, MD; Ronghu Wu, PhD; Khalid Salaita, PhD; Chunhui Xu , PhD

**BACKGROUND:** Anticancer therapies have significantly improved patient outcomes; however, cardiac side effects from cancer therapies remain a significant challenge. Cardiotoxicity following treatment with proteasome inhibitors such as carfilzomib is known in clinical settings, but the underlying mechanisms have not been fully elucidated.

**METHODS AND RESULTS:** Using human induced pluripotent stem cell-derived cardiomyocytes (hiPSC-CMs) as a cell model for drug-induced cytotoxicity in combination with traction force microscopy, functional assessments, high-throughput imaging, and comprehensive omic analyses, we examined the molecular mechanisms involved in structural and functional alterations induced by carfilzomib in hiPSC-CMs. Following the treatment of hiPSC-CMs with carfilzomib at 0.01 to 10  $\mu\text{mol/L}$ , we observed a concentration-dependent increase in carfilzomib-induced toxicity and corresponding morphological, structural, and functional changes. Carfilzomib treatment reduced mitochondrial membrane potential, ATP production, and mitochondrial oxidative respiration and increased mitochondrial oxidative stress. In addition, carfilzomib treatment affected contractility of hiPSC-CMs in 3-dimensional microtissues. At a single cell level, carfilzomib treatment impaired  $\text{Ca}^{2+}$  transients and reduced integrin-mediated traction forces as detected by piconewton tension sensors. Transcriptomic and proteomic analyses revealed that carfilzomib treatment downregulated the expression of genes involved in extracellular matrices, integrin complex, and cardiac contraction, and upregulated stress responsive proteins including heat shock proteins.

**CONCLUSIONS:** Carfilzomib treatment causes deleterious changes in cellular and functional characteristics of hiPSC-CMs. Insights into these changes could be gained from the changes in the expression of genes and proteins identified from our omic analyses.

**Key Words:** cardiomyocyte ■ cardiotoxicity ■ drug research ■ gene expression ■ stem cell

Anticancer therapies have significantly improved the outcomes of patients with cancer over the past decade. However, several common chemotherapeutic agents, including proteasome inhibitors, are associated with an increased risk of arrhythmias, conduction abnormalities, and other cardiac adverse events. Cardiac toxicities have been reported with Food and Drug Administration–approved proteasome inhibitors in clinical trials.<sup>1</sup> Carfilzomib, a

second-generation proteasome inhibitor for the treatment of relapsed or refractory multiple myeloma, can cause cardiotoxicity.<sup>1–4</sup> Clinical trials with carfilzomib have indicated cardiotoxicity including heart failure and cardiac arrhythmias.<sup>5–7</sup> A meta-analysis of 29 clinical trials including 4164 patients who received carfilzomib reported 8.6% and 4.9% incidence of all-grade and high-grade cardiotoxicity, respectively.<sup>8</sup> Another meta-analysis of 24 clinical trials including 2594 patients

Correspondence to: Chunhui Xu, PhD, Emory University School of Medicine, 2015 Uppergate Drive, Atlanta, GA 30322. E-mail: chunhui.xu@emory.edu  
For Sources of Funding and Disclosures, see page 26.

© 2021 The Authors and Emory University school of Medicine. Published on behalf of the American Heart Association, Inc., by Wiley. This is an open access article under the terms of the Creative Commons Attribution-NonCommercial License, which permits use, distribution and reproduction in any medium, provided the original work is properly cited and is not used for commercial purposes.

JAHA is available at: [www.ahajournals.org/journal/jaha](http://www.ahajournals.org/journal/jaha)

## CLINICAL PERSPECTIVE

### What Is New?

- Treatment of human stem cell-derived cardiomyocytes with carfilzomib resulted in oxidative stress, mitochondrial dysfunction, and cell death.
- Carfilzomib treatment negatively affected contractility, Ca<sup>2+</sup> handling, and integrin-mediated traction forces in human stem cell-derived cardiomyocytes.
- Carfilzomib treatment downregulated the expression of genes involved in extracellular matrices, integrin complex, and cardiac contraction and upregulated stress responsive proteins.

### What Are the Clinical Implications?

- Improving mitochondrial function, Ca<sup>2+</sup> handling, cardiac contraction, and integrin-mediated traction forces has the potential to mitigate carfilzomib-induced cardiotoxicity.
- The molecules such as heat shock proteins upregulated by carfilzomib treatment are potential biomarkers for carfilzomib-induced cardiotoxicity.

## Nonstandard Abbreviations and Acronyms

<b>3D</b>	3-dimensional
<b>DMSO</b>	dimethyl sulfoxide
<b>ECM</b>	extracellular matrix
<b>GO</b>	gene ontology
<b>hiPSC-CMs</b>	human induced pluripotent stem cell-derived cardiomyocytes
<b>HSPs</b>	heat shock proteins
<b>RNA-seq</b>	RNA sequencing
<b>ROS</b>	reactive oxygen species
<b>TGT</b>	tension gauge tether

who received carfilzomib showed 18.1% and 8.2% incidence of all-grade and high-grade cardiotoxicity, respectively.<sup>9</sup> Although carfilzomib is used frequently in the treatment of multiple myeloma, the incidence of cardiotoxicity caused by carfilzomib appears to be higher than other proteasome inhibitors.<sup>8</sup>

Carfilzomib has been well-characterized for its potent activity to irreversibly bind to and inhibit the chymotrypsin-like site of the proteasome,<sup>10</sup> blocking the ability of the ubiquitin/proteasome system to degrade and recycle misfolded or damaged proteins.<sup>11</sup> Carfilzomib can effectively induce apoptosis and kill multiple types of human cancer cells with IC<sub>50</sub> ranging from 50 to 300 nM/L after 24 hours exposure of cell cultures to carfilzomib.<sup>12</sup> Cardiomyocytes are also sensitive to proteasome

inhibition possibly because of high protein turnover of contractile proteins.<sup>11</sup> For example, exposure of primary neonatal rat cardiomyocytes to submicromolar concentrations of carfilzomib induced apoptosis and myocyte damage.<sup>13</sup> A preclinical pharmacokinetics study identified chymotrypsin-like proteasomal activity of carfilzomib that can potentially damage rat cardiomyocytes at clinically relevant concentrations.<sup>14</sup> However, cellular and molecular mechanisms underlying carfilzomib-induced cardiotoxicity remain to be fully elucidated.

Because cardiovascular side effects of cancer therapies are increasing, the development of a human cell model is needed to facilitate the understanding of cardiotoxicity-related mechanisms. Progress in hiPSC-CM research has provided a new platform for the studies of drug-induced side effects and disease modeling.<sup>15,16</sup> hiPSC-CMs have translational potential to improve current models by providing more precise and clinically relevant characteristics on responses to drug treatment.<sup>17</sup> They can also overcome the differences between human and animal cardiac physiology and challenges in long-term maintenance of primary human cardiomyocytes and can be engineered for scalable manufacture. hiPSC-CMs have provided novel insights for the study of genetic heart diseases and drug responses.<sup>18–20</sup> Patient-specific hiPSC-CMs have also been used for pharmacogenetic studies to facilitate the identification of cancer survivors with increased risk of chemotherapy-related cardiomyopathy.<sup>21</sup>

To advance our understanding of the underlying mechanisms contributing to the carfilzomib-induced cardiotoxicity, here we provide a molecular and functional view of hiPSC-CMs after carfilzomib treatment. We found that carfilzomib induced dose-dependent cytotoxicity and targeted mitochondria at physiologically relevant doses, leading to the disruption of cellular energy and contractility. Additionally, we examined cellular function at the single cell level through traction force measurements using a nucleic acid-based tension sensor along with Ca<sup>2+</sup> transient imaging. Our findings on reduction in traction forces, abnormal Ca<sup>2+</sup> transients, mitochondrial dysfunction, and contractility impairment, in combination with comprehensive transcriptome and proteome analyses, illustrate the possible molecular mechanisms in cardiomyocyte functional alteration after carfilzomib treatment. Our study also provides a unique resource for the discovery of biomarkers associated with cardiomyocyte dysfunction and arrhythmias following carfilzomib therapy.

## METHODS

### Data Availability

Global gene expression profiling of RNA sequencing (RNA-seq) data are available at the National Center for

Biotechnology Information Gene Expression Omnibus database with the accession number GSE163102. The proteomics data were deposited in the public MassIVE database with the identifier MSV000087350. Institutional review board approval was not required, because this study did not involve the use of animals or human subjects.

## Cardiomyocyte Differentiation and Spheroid Formation

Human induced pluripotent stem cell lines SCVI-273 (Stanford Cardiovascular Institute) and IMR-90 (WiCell Research Institute) were differentiated toward cardiomyocytes using small molecules or growth factors based on previously published differentiation protocols<sup>22,23</sup> (Figure 1A). Human induced pluripotent stem cell monolayers were dissociated using Versene (Thermo Fisher Scientific) and seeded onto 12-well plates coated with 1:60 Matrigel (Thermo Fisher Scientific). Cardiomyocyte differentiation was performed using 6  $\mu\text{mol/L}$  CHIR 99021 (Selleck Chemicals) in RPMI/B27 insulin-free medium (days 0–1) followed by 5  $\mu\text{mol/L}$  IWR-1 (Sigma-Aldrich) for 2 days on days 3 to 5. Medium was changed on day 5, and cells were maintained in RPMI/B27 with insulin for the remaining of days. In the second protocol, cells were treated with 100 ng/mL recombinant human activin A (R&D Systems) on day 0 and replaced with 10 ng/mL recombinant human bone morphogenic protein-4 (R&D Systems) in RPMI/B27 insulin-free medium from days 1 to 4. Differentiated cells were maintained in RPMI/B27 with insulin for 5 weeks with medium change every 2 to 3 days. Spheroids were generated using AggreWell400 plates (1800 cells per microwell for each spheroid) from differentiated cultures on differentiation day 6 and maintained in RPMI/B27 with insulin.

SCVI-273 hiPSC-CMs were used for oxidative stress, caspase activity, mitochondrial membrane potential, ATP measurement,  $\text{Ca}^{2+}$  transients, measurements of sarcomere length and cell structure, and RNA-seq analysis. IMR-90 hiPSC-CMs were used for quantitative reverse transcription–polymerase chain reaction, traction force, contractility, and proteomics analysis. Both hiPSC lines SCVI-273- and IMR90-derived CMs were used for cell viability and mitochondrial function with similar results, and data from SCVI-273 hiPSC-CMs were presented.

## Assay to Determine Mitochondrial Membrane Potential

To analyze changes in mitochondrial membrane potential in hiPSC-CMs, we used tetramethyl rhodamine methyl ester, a dye probe that accumulates in mitochondria. Medium was removed following 1-day

treatment with carfilzomib, and cells were labeled with 100 nmol/L tetramethyl rhodamine methyl ester for 30 minutes at 37 °C. Cells were then counter stained with Hoechst (Thermo Fisher Scientific; H3570) and imaged immediately using ArrayScan XTI Live High Content Platform (Life Technologies).<sup>24</sup> We quantified the nuclear spots within the ring in channel 2 by using intensity as a readout.

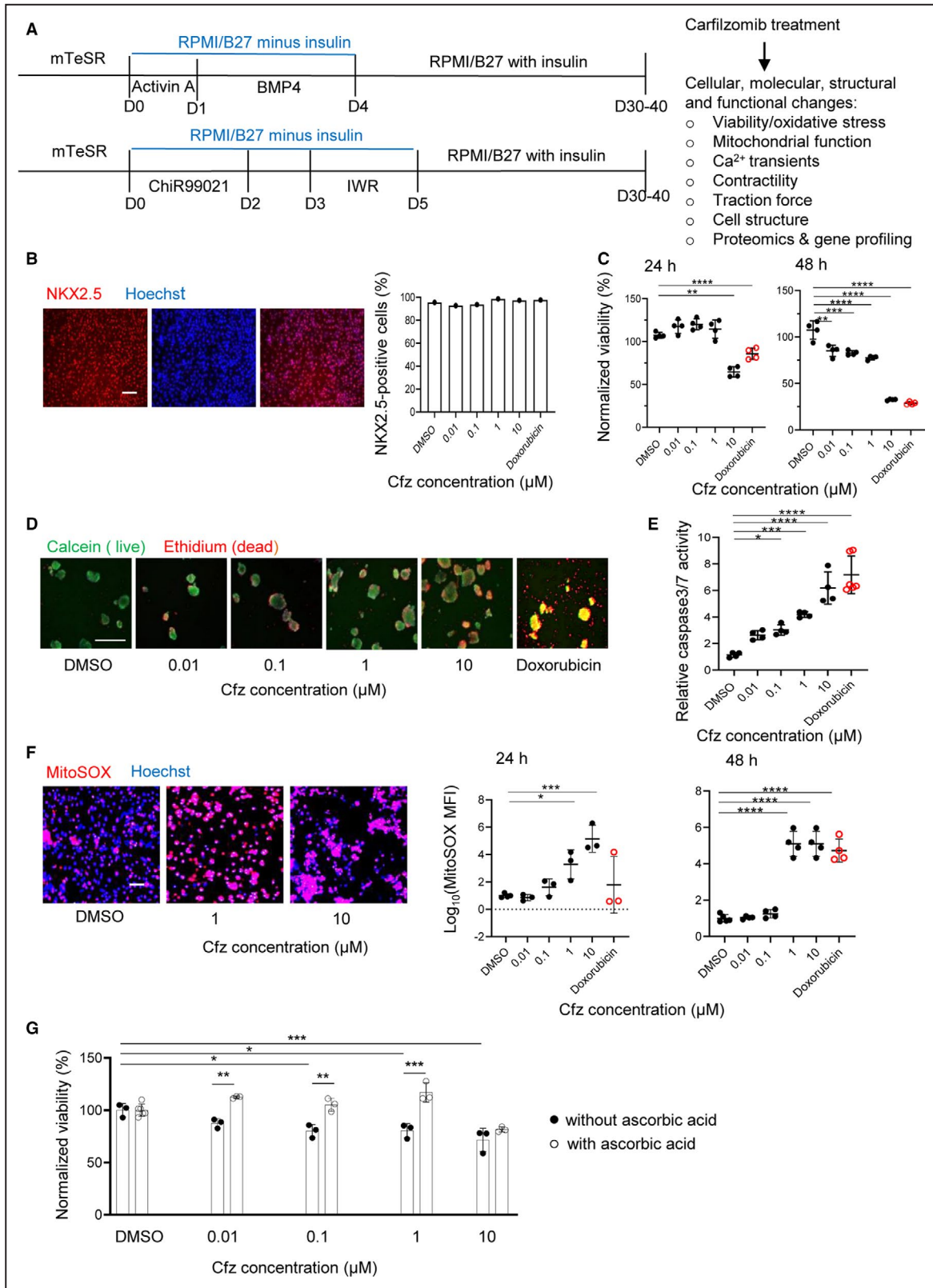
## Drug Preparation and Treatment

The stock solution of 10 mmol/L carfilzomib (Selleck Chemicals; PR-171 and S2853) was prepared by dissolving 10 mg carfilzomib in 1.389 mL dimethyl sulfoxide (DMSO; Sigma-Aldrich) and stored at  $-80$  °C. The peak plasma concentration based on pharmacokinetic characteristics of carfilzomib is 5.88  $\mu\text{mol/L}$ . A dose range from 0.01 to 10  $\mu\text{mol/L}$  was selected following initial testing of carfilzomib at 1, 2, 10, and 20  $\mu\text{mol/L}$ . To make  $\times 2$  final concentration of carfilzomib in RPMI/B27 with insulin, drug dilution was performed on the day of each experiment and kept on ice in the dark. DMSO at 0.2% (v/v), a concentration corresponding to the highest drug concentration, was used as vehicle control. Doxorubicin (Adriamycin; Selleck Chemicals) at 10  $\mu\text{mol/L}$  was used as a positive control for viability testing and 1  $\mu\text{mol/L}$  for contractility and  $\text{Ca}^{2+}$  transient analysis. Stock solution of doxorubicin (10 mmol/L) was made in the same manner as carfilzomib. The peak plasma concentration of doxorubicin is 1.8 to 11  $\mu\text{mol/L}$ .

For the rescue experiment, hiPSC-CMs were pre-treated with ascorbic acid (Sigma-Aldrich) at 25  $\mu\text{g/mL}$  for 2 hours before the carfilzomib treatment and then treated with carfilzomib and ascorbic acid for 24 hours before the analysis of cell viability by CellTiter-Blue assay (Promega). All treatments were adjusted to equivalent concentrations of DMSO (solvent).

## In Vitro Cytotoxicity Assays

For monolayer culture of hiPSC-CMs, cell viability was measured using CellTiter-Blue assay (Promega). Monolayer cultures of hiPSC-CMs (IMR-90 and SCVI-273) were plated in Matrigel (1/60)-coated 96-well plates with clear bottom and black wall. Cells were allowed to attach at 37 °C in RPMI-B27 with Rock inhibitor (10  $\mu\text{mol/L}$ ) for 24 hours before treatment with carfilzomib. Serially diluted carfilzomib was added to cells. After 24 and 48 hours of carfilzomib treatment, cells were incubated with 20  $\mu\text{L}$  of the CellTiter-Blue reagent in 100  $\mu\text{L}$  of RPMI/B27 medium solution for 2 hours, and the reduction of resazurin to resorufin in live cells was measured by fluorescence excitation at 530 nm and emission at 590 nm using a BioTek micro-plate reader and Gen5 3.03 software. For 3-dimensional (3D) hiPSC-CMs, cell viability was measured by Live/Dead staining



(Thermo Fisher Scientific). A master mix of 1 μmol/L ethidium homodimer and 0.25 μmol/L of calcein in RPMI/B27 medium was added following a wash with PBS.

Cells were incubated for 25 minutes at 37 °C, washed twice with PBS, and suspended in 5 mL of RPMI/B27 medium without phenol red. Live/dead-stained cells



**Figure 1. Cfz treatment-induced dose-dependent cytotoxicity in human induced pluripotent stem cell-derived cardiomyocytes (hiPSC-CMs).**

**A**, Overall experimental design. **B**, Representative images of immunofluorescence staining for examining cardiac purity using NKX2.5 antibodies and cardiomyocyte purity (percent NKX 2.5-positive cells) of 3-dimensional (3D) hiPSC-CMs following the treatment with Cfz analyzed by ArrayScan. **C**, Relative cell viability of hiPSC-CMs 24 and 48 hours after Cfz treatment measured by CellTiter-Blue fluorescence assay (n=4 cultures). **D**, Cell viability of 3D hiPSC-CMs 24 hours after Cfz treatment using Live/Dead staining (red ethidium-stained cells were dead cells; green calcein-stained cells were live cells). Scale bar=100  $\mu$ m. **E**, Relative caspase3/7 activity of hiPSC-CMs 48 hours after Cfz treatment (n=4–5 cultures). **F**, Representative images of MitoSOX staining and summary of MitoSOX MFI in hiPSC-CMs 24 and 48 hours after Cfz treatment (n=3–4 cultures). Nuclei were counterstained with Hoechst. Scale bar=50  $\mu$ m. **G**, Relative cell viability of hiPSC-CMs 24 hours following Cfz treatment with and without ascorbic acid (n=3 cultures). hiPSC-CMs were pretreated with ascorbate acid for 2 hours, followed by cotreatment with Cfz for 24 hours. Cfz indicates carfilzomib; D, day; DMSO, dimethyl sulfoxide; h, hour; and MFI, mean fluorescence intensity. \* $P$ <0.05; \*\* $P$ <0.01; \*\*\* $P$ <0.001; \*\*\*\* $P$ <0.0001.

were observed at 645 nm for ethidium homodimer and 530 nm for calcein-acetoxymethyl ester.

### Immunofluorescence Staining

hiPSC-CMs were dissociated with 0.05% Trypsin-EDTA and reseeded in Matrigel-coated 96-well culture plates at a density of  $5 \times 10^4$  cells per well. Retrieved cells were fixed in 4% paraformaldehyde for 15 minutes following gentle PBS wash and permeabilized using 90% cold methanol for 2 minutes at room temperature. The cells were then blocked with 10% normal goat serum in PBS at room temperature for 1 hour and incubated overnight at 4 °C with the primary antibodies against NKX2.5 (Cell Signaling; 1:1600) and  $\alpha$ -actinin (Sigma-Aldrich; 1:800) diluted in 3% normal goat serum for the purity assay.<sup>23</sup> After the incubation with the primary antibodies, the cells were washed twice with PBS and incubated with secondary antibodies, Alexa Fluor 488-conjugated goat anti-mouse immunoglobulin G1 (for  $\alpha$ -actinin staining, Life Technologies) and Alexa Fluor 594-conjugated goat anti-rabbit immunoglobulin G (for NKX2.5 staining; Life Technologies) diluted at 1:1000 in PBS with 0.25% BSA. The nuclei were counterstained with 7  $\mu$ mol/L Hoechst33342 (Thermo Fisher Scientific) for 15 minutes at room temperature and preimaged using an inverted microscope (Axio Vert.A1). Images of immunocytochemistry were quantitatively analyzed using ArrayScan XTI Live High Content Platform. The Cellomics Scan Software (Thermo Fisher Scientific) was used to capture images, and data analysis was performed using Cellomics View Software (Thermo Fisher Scientific). Twenty fields per well were imaged using a  $\times 10$  objective. Spot threshold was set to 10 units, and detection limit was set at 25 units. The percentage of  $\alpha$ -actinin-positive cells and the average intensity per well were used as a readout.

### Caspase 3/7 Detection

Fresh Caspase-GloR 3/7 reagent (Promega) was reconstituted and added to cells as an indicator of apoptosis. Background readings were measured from wells

containing culture medium without cells. Illuminometer readings were taken 1 hour after adding the Caspase-GloR 3/7 reagent.

### Assay to Measure ATP Content

CellTiter-Glo 3D Cell Viability kit (Promega) was used to detect alterations in the cellular ATP content. 3D hiPSC-CMs were dissociated into single cells using 0.25% Trypsin-EDTA and replated into a 96-well plate at a density of  $4.5 \times 10^4$  cells per well. Medium was removed, and RPMI without phenol red was added at 100  $\mu$ L per well. The kit was thawed at 4 °C a day before and the reagent was added at 100  $\mu$ L per well (1:1 ratio) with 2 minutes shaking. Measurement was performed at Top Count NXT Microplate Luminescence Counter (PerkinElmer) with integration time of 1 second per well after 20 minutes incubation in room temperature.

### Quantitative Reverse Transcription-Polymerase Chain Reaction

Total RNA was extracted using Aurum total RNA mini kit (Bio-Rad) according to manufacturer's instructions. One microgram total RNA was used for complementary DNA synthesis using the Superscript VILO complementary DNA synthesis kit (Thermo Fisher Scientific), and reaction mixture was incubated using a C1000 touch thermal cycler (Bio-Rad) as follows: 25 °C for 10 minutes, 37 °C for 2 hours and 85 °C for 5 minutes. The reaction mixture was further diluted to 300 and 2  $\mu$ L complementary DNA as the template was subjected to quantitative reverse transcription-polymerase chain reaction, which was performed in triplicate for each gene using a SYBR Green reaction master mix (Bio-Rad). Real-time polymerase chain reaction conditions included initial denaturation step at 95 °C for 10 minutes, 40 cycles of 2-steps with 15 seconds of denaturation at 95 °C, followed by 1 minutes of annealing at 60 °C using Applied Biosystems 7500 real-time polymerase chain reaction systems. The messenger RNA levels of the genes examined were normalized to GAPDH messenger RNA levels. The primers used for the genes are listed in Table 1.

**Table 1. Primers for Quantitative Reverse Transcription–Polymerase Chain Reaction**

Gene	Description of full name	Accession code	Primer
<i>ATP2A2</i>	ATPase, Ca <sup>2+</sup> transporting, cardiac muscle, slow twitch 2	NM_170665	Forward: TCAGCAGGAACCTTTGTCCACC Reverse: GGGCAAAGTGATCGACAGG
<i>CASQ2</i>	Calsequestrin 2	NM_001232	Forward: TTATGTTCAAGGACCTGGGC Reverse: GCCTCTACTACCATGAGCCG
<i>GAPDH</i>	Glyceraldehyde-3-phosphate dehydrogenase	NM_001256799	Forward: CTGGGCTACACTGAGCACC Reverse: AAGTGGTCGTTGAGGGCAATG
<i>MYH6</i>	Myosin, heavy chain 6, cardiac muscle, alpha (α-MHC)	NM_002471	Forward: CTTCTCCACCTTAGCCCTGG Reverse: GCTGGCCCTTCAACTACAGA
<i>MYL2</i>	Myosin, light chain 2, regulatory, cardiac, slow (MLC-2V)	NM_000432	Forward: CGTTCTTGCAATGAAGCCA Reverse: CAACGTGTTCTCCATGTTCCG
<i>RYR2</i>	Ryanodine receptor 2, cardiac	NM_001035	Forward: CAAATCCTTCTGCTGCCAAG Reverse: CGAAGACGAGATCCAGTTCC
<i>SLC8A1</i>	Solute carrier family 8 (sodium/calcium exchanger), member 1	NM_021097	Forward: CTGGAATTCGAGCTCTCCAC Reverse: ACATCTGGAGCTCGAGGAAA
<i>OPA1</i>	OPA1 mitochondrial dynamin like GTPase	NM_015560.3	Forward: TGAAGCATCAAGTTTTTCTTG Reverse: TGCTGAAGATGGTGAGAAGAAG
<i>NDUFB5</i>	NADH ubiquinone oxoreductase subunit B5	NM_002492.4	Forward: ATGGTCTCCACTGTGTGAA Reverse: GGTGGCAGCTCTGTCTGG
<i>MFN2</i>	Mitofusin 2	NM_014874.4	Forward: TTGCATCGAGAGAAGAGCAG Reverse: GTCTTTTGGACTTCAGCCAT
<i>MFN1</i>	Mitofusin 1	NM_033540.3	Forward: GTTTTCACTGCTGACTGCGA Reverse: GTGGCACTTGTGAAGGATT
<i>COQ10A</i>	Coenzyme Q10 homolog A	NM_144576	Forward: CTTACCTTCGAGCCGTTCTT Reverse: CCATGATTCTACGCTCCGAGTA
<i>UCP3</i>	Uncoupling protein 3	NM_003356.4	Forward: AACGCAAAAAGGAGGGTGTA Reverse: CTCCAGGCCAGTACTTCAGC

Primers were retrieved from open access websites (<http://primerdepot.nci.nih.gov/> or <http://pga.mgh.harvard.edu/primerbank/>).

## Detection of Mitochondrial Reactive Oxygen Species

To analyze changes in mitochondrial reactive oxygen species (ROS), we used MitoSOX Red (Thermo Fisher Scientific) staining. The cells were washed with PBS and incubated with 5 μmol/L MitoSOX Red for 15 minutes at 37 °C and protected from light. Cells were counter-stained with Hoechst (Thermo Fisher Scientific) and imaged using ArrayScan XT Live High Content Platform (Life Technologies).

## Seahorse Extracellular Flux Analysis of Mitochondrial Respiration

Seahorse plates were coated with Matrigel at 1:50 dilution 1 day before cell seeding. hiPSC-CMs were seeded at 2.5×10<sup>5</sup> cells per well in 300 μL of the medium and were allowed to adhere for 1 day in a 37 °C humidified incubator with 5% CO<sub>2</sub>. The Seahorse XF Sensor Cartridge was hydrated the day before by filling each well of the XF Utility plate with 1 mL of Seahorse XF Calibrant Solution and kept in a non-CO<sub>2</sub> 37 °C incubator for 24 hours to remove CO<sub>2</sub> from the media to prevent interference with pH-sensitive measurements. To pre-equilibrate, hiPSC-CMs were washed

once with nonbuffered RPMI supplemented with 10 mmol/L glucose, 2 mmol/L sodium pyruvate, and 2 mmol/L glutamine. Cells were maintained in 525 μL of XF Assay medium at 37 °C in a non-CO<sub>2</sub> incubator for 1 hour. Agilent Seahorse XF24 Analyzer (Agilent Seahorse Bioscience) was used to analyze the mitochondrial function of the cells by sequential injections of modulators. A mixture of oligomycin (2 μmol/L), carbonyl cyanide-4-(trifluoromethoxy) phenylhydrazide (1 μmol/L), and rotenone (0.5 μmol/L) were suspended in a prewarmed XF Assay medium and loaded into the injection ports (75 μL) of the hydrated sensor cartridge corresponding to the order of injection. Each measurement cycle consisted of 3 minutes of mixing, 2 minutes of waiting, and 3 minutes of measurements of oxygen consumption respiration. Measurement cycles were performed after each addition of the given compounds. The data were analyzed using Wave 2.6 and Report Generator Version: 4.0.

## Ca<sup>2+</sup> Transient Imaging

Live cell imaging of intracellular Ca<sup>2+</sup> transients was performed with dye Fluo-4 AM (Thermo Fisher Scientific). Cells were incubated in Tyrode solution<sup>25</sup> containing

Fluo-4 AM at a final concentration of 10  $\mu\text{mol/L}$  in the dark at 37 °C for 20 minutes followed by a gentle wash at room temperature in prewarm Tyrode solution. Fluorescence images were acquired using the Image Xpress Micro XLS System (Molecular Devices) with excitation/emission at 488/515 to 600 nm at a rate of 5 frames per second and  $\times 10$  magnification for 4 fields per well.

### Video-Based Contractility Measurement

Contractility of spontaneously beating hiPSC-CMs was recorded using a phase-contrast inverted microscope (Axio Vert.A1) equipped with Zeiss Axio Cam digital camera system.

Videos were recorded for 30 seconds (5 frames/s) under  $\times 10$  magnification and were processed and exported using Zeiss AxioVision LE imaging software. Videos were converted to frame by frame image sequence using ImageJ (National Institutes of Health). Video-based analysis of contractility was performed using MATLAB and motion vector software (R2016b; MathWorks).<sup>26</sup>

### Probe Preparation and Traction Force Measurement

Turn on tension gauge tether (TGT) probes were used to measure molecular traction forces. DNA duplexes were conjugated to the fibronectin mimic cyclic-Arg-Gly-Asp-*Phe*-Lys (*Phe* is *D* isomer) (cRGDfK), fluorophore (Cy3B), and quencher (BHQ) using previously published protocols.<sup>27,28</sup> The duplex was tethered to a surface using biotin-streptavidin binding. When integrin receptors apply sufficient tension, the duplex will mechanically denature and specifically when the applied force exceeds the tension tolerance of the probe. The shearing TGT with a tension tolerance of 56 pN was used as described previously.<sup>29</sup> Glass surfaces were activated and functionalized with streptavidin. Next, biotinylated DNA tension probes were added. 3D hiPSC-CMs were treated with carfilzomib for 1 day, dissociated, and then reseeded on the DNA-modified glass surfaces. Microscopy imaging of spontaneously contracting cells was performed using a Nikon TIRF microscope with  $\times 100$  objectives.

### Measurements of Sarcomere Length and Cell Structure

3D-derived hiPSC-CMs were treated with carfilzomib for 1 day, and then dissociated and reseeded on the glass-bottom microplates. Cells were stained with antibodies against  $\alpha$ -actinin, and microscopy imaging was performed using a Nikon TIRF microscope in

reflection interference contrast microscopy and TRITC channels with  $\times 100$  objectives. ImageJ software was used to quantify cell morphology, cell spread area, circularity, and aspect ratio. A program was written to obtain automated outlining of cells. To measure the z-lines, individual z-lines were selected, and lengths were measured per cell. For each cell, the average length of  $\approx 20$  to 30 z-lines was plotted.

### RNA Sequencing

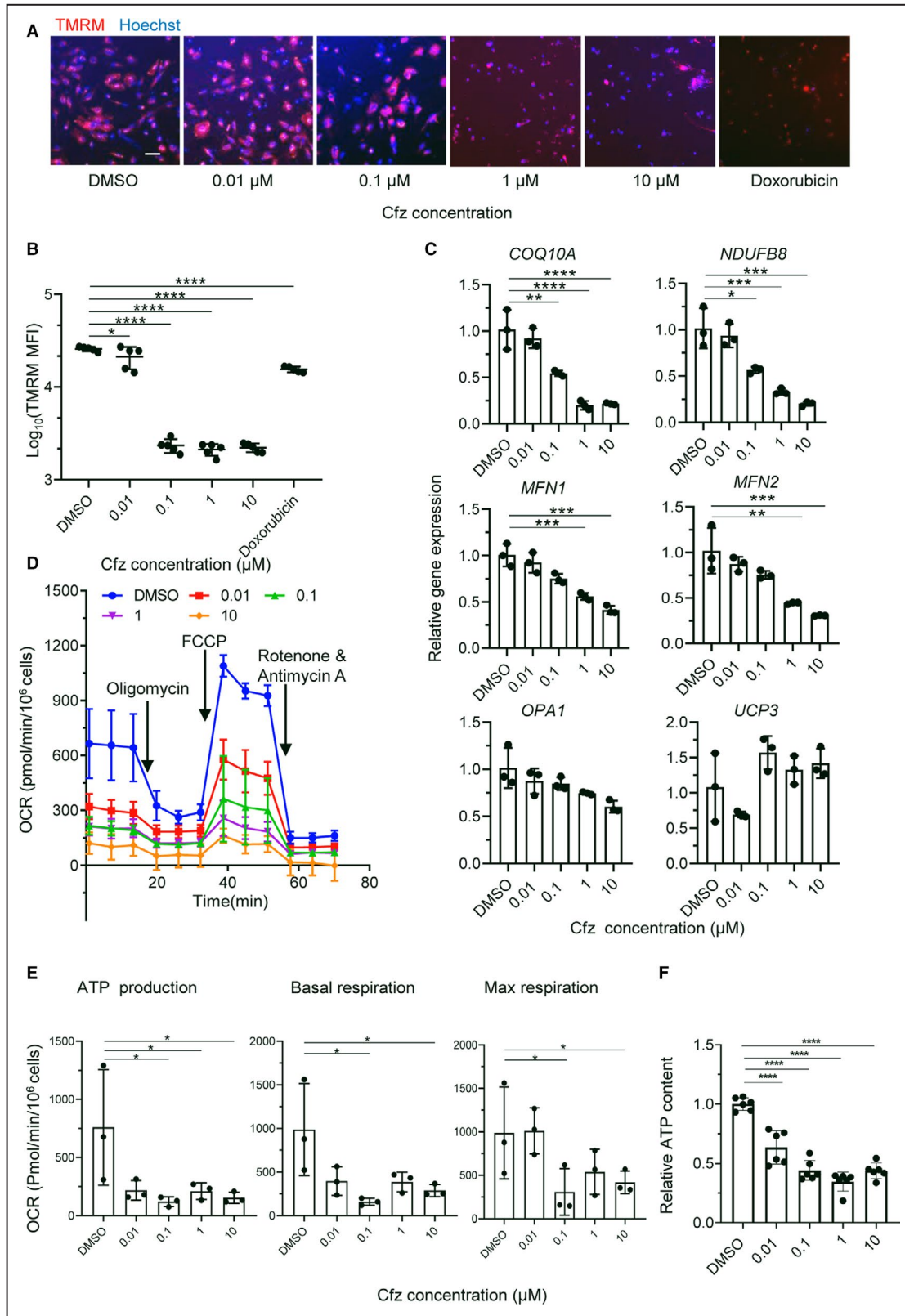
Total RNA was isolated from day 30 hiPSC-CMs in biological triplicates following 1 day of carfilzomib treatment using Aurum total RNA mini kit (Bio-Rad) according to the manufacturer's instructions. RNA concentrations were measured using Nanodrop Spectrophotometer (Thermo Fisher Scientific). Library preparation and RNA-seq was conducted by Novogene with 20 M reads per sample, PE150 Mapped Homo sapiens (GRCh38/hg38) to the genome using STAR (v2.6.1d) with ensemble annotation. Fastp was used for length limitation of adapter trimming (<https://github.com/novogene-europe/fastp>). The differentially expressed genes were used for analyses of gene ontology (GO) terms and *Kyoto Encyclopedia of Genes and Genomes* pathways, which were considered significantly enriched if the adjusted  $P < 0.05$ .

### Proteomic Analysis

Cells and culture media were collected from the triplicates of 3D hiPSC-CM cultures following 1 day of carfilzomib treatment. Proteins were extracted from 3 to  $4 \times 10^6$  hiPSC-CMs per sample by suspending the cells in the lysis buffer as described previously.<sup>30</sup> Proteins were purified through methanol-chloroform precipitation. For the secretome analysis, the media was passed through a filter (0.45  $\mu\text{m}$ ) and then concentrated by centrifugation (molecular weight 3 kDa cutoff). Proteins were digested with trypsin overnight. Then, purified peptides were labeled with the 6-plex tandem mass tag reagents for protein quantitation. The tandem mass tag-labeled samples (6 for the cell lysates and 6 for the secretomes) were mixed and fractionated. Each fraction was analyzed by liquid chromatography-tandem mass spectrometry. The data analyses were conducted as reported previously.<sup>30</sup>

### Statistical Analysis

Statistical analyses were done using GraphPad Prism version 8.00. Global differences were evaluated by Dunnett and Turkey test (1-way ANOVA).  $P < 0.05$  was taken as statistically significant. Results are presented as mean  $\pm$  SD in all experiments. Sample sizes are indicated



in figure legends. For group comparison of gene expression in RNA-seq analysis, Benjamin-Hochberg correction was used to control false-discovery rate.

We considered genes to be significantly differentially expressed between the two groups if adjusted  $P < 0.05$  and absolute value of  $\log_2$  (fold change)  $> 1$ .



**Figure 2. Cfz treatment reduced mitochondrial function of human induced pluripotent stem cell-derived cardiomyocytes (hiPSC-CMs).**

**A**, Measurement of TMRM fluorescence 24 hours after Cfz treatment. Nuclei were counterstained with Hoechst. Scale bar=100  $\mu$ m. **B**, Summary of TMRM MFI analyzed by ArrayScan (n=5 cultures). **C**, Effects of Cfz treatment on the expression of genes related to mitochondrial function in hiPSC-CMs (n=3 cultures). Gene expression is normalized to the housekeeping gene *GAPDH* and shown as relative levels to the control (DMSO treated) group. **D**, Representative traces of oxygen consumption rate recording in hiPSC-CMs upon sequential treatments with oligomycin, FCCP, and a mixture of rotenone and antimycin A. **E**, Quantification of ATP production, basal respiration, and maximal respiration (n=4 cultures). The results were normalized to  $1 \times 10^6$  cells. **F**, Relative cellular ATP content in 3-dimensional hiPSC-CMs 24 hours after Cfz treatment as measured by an ATP-based luminescence assay (n=5 cultures). \* $P < 0.05$ ; \*\* $P < 0.01$ ; \*\*\* $P < 0.001$ ; \*\*\*\* $P < 0.0001$ . Cfz indicates carfilzomib; *COQ10A*, coenzyme Q10A; DMSO, dimethyl sulfoxide; FCCP, carbonyl cyanide-4-(trifluoromethoxy) phenylhydrazine; MFI, mean fluorescence intensity; *MFN1*, mitofusin 1; *MFN2*, mitofusin 2; *NDUFB8*, NADH:ubiquinone oxidoreductase subunit B8; OCR, oxygen consumption rate; *OPA1*, OPA1 mitochondrial dynamin like GTPase; TMRM, tetramethyl rhodamine methyl; and *UCP3*, uncoupling protein 3.

## RESULTS

### Carfilzomib Treatment Induced a Dose- and Duration-Dependent Cardiotoxicity

To examine whether carfilzomib treatment causes cytotoxicity in hiPSC-CMs, we generated enriched hiPSC-CMs (>90% NKX2.5-positive cells), treated the cells with various doses of carfilzomib, and characterized the cells 24 and 48 hours after treatment (Figure 1A and 1B). We used a common chemotherapeutic drug, doxorubicin, at 10  $\mu$ mol/L (a peak plasma concentration) as a control.<sup>31</sup> Following carfilzomib treatment, we observed dose- and duration-dependent increase of cell loss in carfilzomib-treated cultures compared with DMSO-treated cultures (Figure 1C). As detected by CellTiter Blue assay, cultures treated with carfilzomib at 10  $\mu$ mol/L and doxorubicin for 24 hours had lower cell viabilities compared with cultures treated with DMSO. The cell viability in cultures treated with carfilzomib for 48 hours began to decrease at doses as low as 0.1  $\mu$ mol/L, which is significantly lower than the peak concentration of the carfilzomib observed in patients' plasma after intravenous administration.<sup>32,33</sup> Given that hiPSC-CM spheroids (3D cultures) provide a more physiologically relevant context for drug toxicity,<sup>34</sup> we examined whether carfilzomib could also induce cytotoxicity in 3D cultures. We generated hiPSC-CM spheroids using microscale tissue engineering<sup>23</sup> and treated them with carfilzomib for 24 hours. Using calcein and ethidium bromide as indicators for live and dead cells, respectively, we found that cultures treated with carfilzomib at 10  $\mu$ mol/L and doxorubicin had increased dead cells (ethidium bromide-positive cells), whereas moderate toxicity was also observed in cultures treated with carfilzomib at 0.1 and 1  $\mu$ mol/L (Figure 1D). These results suggest that carfilzomib induced dose-dependent cytotoxicity in both 2-dimensional and 3D cultures.

To determine the mechanism of cell death, we examined caspase3/7 activity using Caspase-Glo 3/7 Luminescent assay. Increased caspase3/7 activation

was detected after carfilzomib treatment for 24 hours, indicating that carfilzomib-induced cytotoxicity might be the result of apoptosis (Figure 1E).

### Carfilzomib Treatment Increased Mitochondrial Superoxide and Reduced Mitochondrial Function of hiPSC-CMs

Oxidative stress through generation of mitochondrial superoxide and mitochondrial dysfunction plays important roles in cellular cytotoxicity,<sup>35,36</sup> which could affect cardiac function.<sup>37-39</sup> We therefore examined the effect of carfilzomib treatment on mitochondrial oxidative stress and mitochondrial function. Based on fluorescence intensity of MitoSOX, a mitochondrial superoxide indicator, the relative levels of mitochondrial superoxide were higher in cultures treated with carfilzomib at 1 and 10  $\mu$ mol/L compared with DMSO-treated cultures (Figure 1F).

To examine if carfilzomib induced cytotoxicity through oxidative stress, we evaluated if ascorbic acid, a commonly used antioxidant, could rescue carfilzomib-induced cell loss. Compared with carfilzomib-treated cultures without ascorbic acid, the carfilzomib-treated cultures with ascorbic acid had significantly attenuated cell loss when cells were treated with carfilzomib at 0.01, 0.1, and 1  $\mu$ mol/L (Figure 1G), suggesting that carfilzomib-induced cytotoxicity is in part mediated by oxidative stress.

We also examined the effect of carfilzomib treatment on mitochondria membrane potential by staining the cells with tetramethylrhodamine methyl ester, a cell-permeant fluorescent dye that is sequestered by active mitochondria. hiPSC-CMs treated with carfilzomib at 0.1, 1, and 10  $\mu$ mol/L had >10-fold reduced levels of tetramethylrhodamine methyl fluorescence intensity (Figure 2A and 2B). These results indicate a substantial decrease in mitochondrial membrane potential and increase in mitochondrial superoxide following carfilzomib treatment, suggesting that oxidative stress could play an important role in carfilzomib-mediated cardiac cytotoxicity.

To understand the effects of carfilzomib on mitochondrial function, we examined the expression of genes associated with mitochondrial function and performed a Seahorse XF Cell Mito stress test 1 day after carfilzomib treatment. Carfilzomib treatment caused a dose-dependent decrease in the expression of genes associated with mitochondrial function, including *COQ10A* (coenzyme Q10A), *MFN1* (mitofusin 1), *MFN2* (mitofusin 2), and *NDUFB5* (NADH:ubiquinone oxidoreductase subunit B8), but not *OPA1* (OPA1 mitochondrial dynamin like GTPase) and *UCP3* (uncoupling protein 3) (Figure 2C). The basal and maximal respiratory capacity and ATP production (serving as an indicator of mitochondrial function) were measured by monitoring oxygen consumption respiration after sequential injection of oligomycin, carbonyl

cyanide-4-(trifluoromethoxy) phenylhydrazine, and rotenone according to the manufacture's instruction. As shown in Figure 2D and 2E, a significant decrease in ATP production was detected following the treatment of carfilzomib at 0.1, 1, and 10  $\mu\text{mol/L}$  in SCVI-273 hiPSC-CMs. The reduced ATP levels were also observed in 3D cultures treated with carfilzomib as detected by CellTiter-Glo viability assay (Figure 2F). Higher concentrations of carfilzomib (10  $\mu\text{mol/L}$ ) also decreased the basal and maximal mitochondrial respiration in SCVI-273 hiPSC-CMs (Figure 2D and 2E). Similarly, carfilzomib treatment reduced ATP production and basal mitochondrial respiration in IMR90 hiPSC-CMs (data not shown). These results suggest that carfilzomib induces mitochondrial damage and consequently the cardiotoxicity.

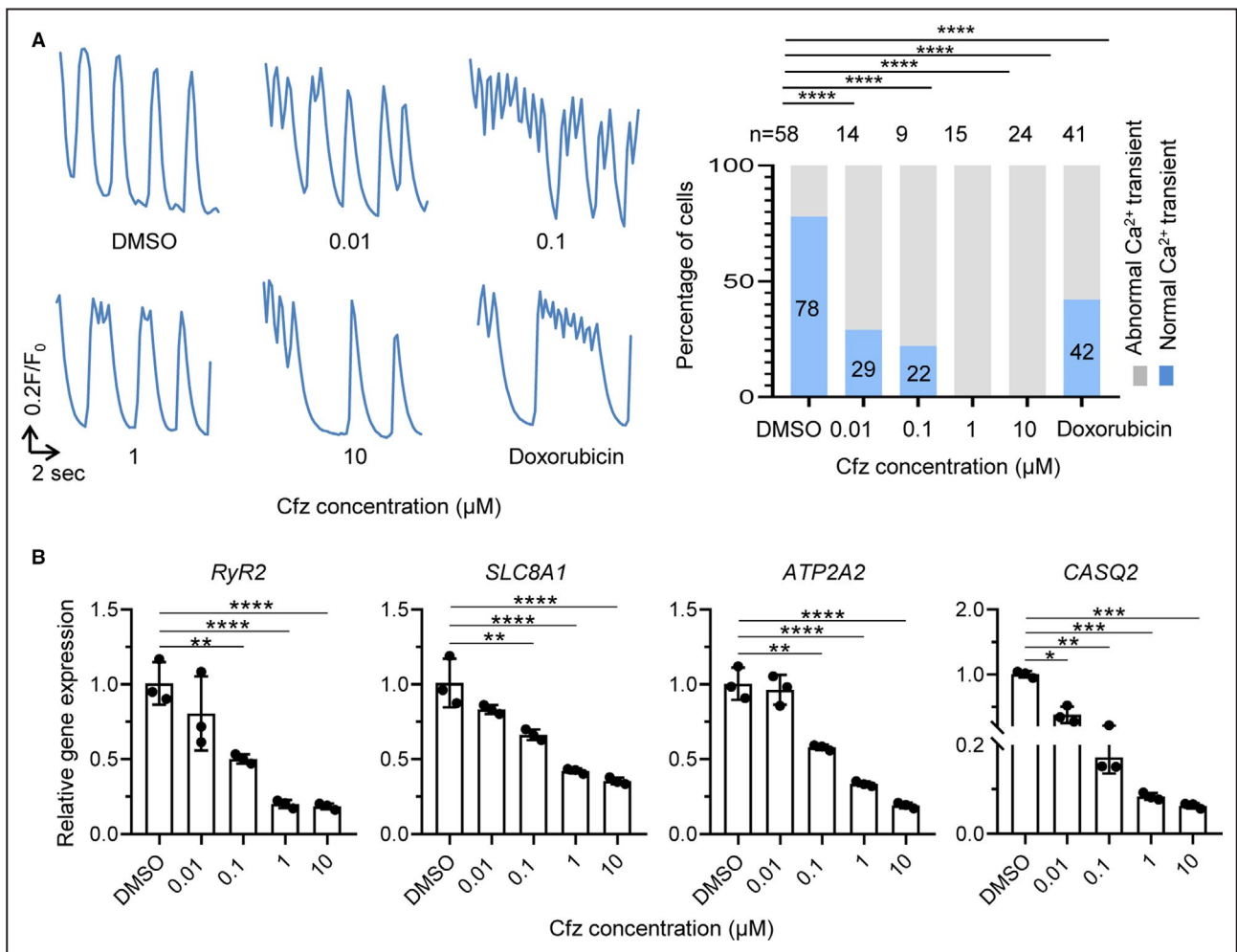


**Figure 3. Czf increased abnormal intercellular Ca<sup>2+</sup> transients of human induced pluripotent stem cell-derived cardiomyocytes (hiPSC-CMs) and decreased the expression of genes associated with Ca<sup>2+</sup> handling.**

**A**, Representative Ca<sup>2+</sup> transient traces from each group and summary of cells with normal and abnormal Ca<sup>2+</sup> transients (n=9–58 cells). hiPSC-CMs were treated with Czf for 24 hours and measured for Ca<sup>2+</sup> transients. Numbers shown on the stack bars represents percentages of cells with normal and abnormal Ca<sup>2+</sup> transients. **B**, Relative expression levels of genes associated with Ca<sup>2+</sup> handling in hiPSC-CMs treated with Czf for 24 hours (n=3 cultures). \*P<0.05; \*\*P<0.01. *ATP2A2* indicates ATPase sarcoplasmic/endoplasmic reticulum Ca<sup>2+</sup> transporting 2; *CASQ2*, calsequestrin 2; Czf, carfilzomib; DMSO, dimethyl sulfoxide; *RyR2*, ryanodine receptor 2; and *SLC8A1*, solute carrier family 8 member A1.

## Carfilzomib Treatment Induced Abnormal $\text{Ca}^{2+}$ Transients and Dysfunctional Contractility

There is increasing evidence that alteration in mitochondrial function results in increased ROS generation and abnormal  $\text{Ca}^{2+}$  transients.<sup>37,40</sup> Considering the link of oxidative stress and  $\text{Ca}^{2+}$  transients, we analyzed the  $\text{Ca}^{2+}$  transient profile 24 hours after carfilzomib treatment. Carfilzomib treatment of SCVI-273 hiPSC-CMs increased the proportion of cells with abnormal  $\text{Ca}^{2+}$  transients (Figure 3A). Consistently, carfilzomib treatment decreased the expression of genes associated with  $\text{Ca}^{2+}$  handling (*SLC8A1* [solute carrier family 8 member A1], *RYR2* [ryanodine receptor 2], *CASQ2* [calsequestrin 2], and *ATP2A2* [ATPase sarcoplasmic/endoplasmic reticulum  $\text{Ca}^{2+}$  transporting 2]) (Figure 3B). The downregulation of these genes is consistent with the abnormal  $\text{Ca}^{2+}$  transients following carfilzomib treatment. These results indicate that carfilzomib treatment impairs  $\text{Ca}^{2+}$  transients at the single cell level, which may affect the contractility function of hiPSC-CMs.

To address if mitochondrial dysfunction along with abnormal  $\text{Ca}^{2+}$  transients was associated with contractile dysfunction in carfilzomib-treated hiPSC-CMs, we assessed the contractility of 3D hiPSC-CM static spheroids after treatment with carfilzomib for 24 and 48 hours using video microscopy with motion vector analysis. Cessations in contraction occurred in cultures treated with all concentrations (0.01, 0.1, 1, and 10  $\mu\text{mol/L}$ ) of carfilzomib for 48 hours. At 24 hours after carfilzomib treatment, a portion of hiPSC-CM spheroids treated with carfilzomib at 0.01  $\mu\text{mol/L}$  or doxorubicin and all spheroids treated with 0.1, 1, and 10  $\mu\text{mol/L}$  stopped beating (Figure 4A). Similar results of cessations in contraction were observed in hiPSC-CMs derived from both SCVI-273 and IMR90 lines treated with carfilzomib at high doses. The average maximum contraction, maximum relaxation velocity, and the beat rate remained unchanged in the remaining beating cells from cultures treated with carfilzomib at 0.01  $\mu\text{mol/L}$  or doxorubicin compared with those from DMSO-treated cultures (Figure 4B and 4C). Additionally, carfilzomib reduced the expression of genes associated with contractility (*MYH6* [myosin heavy chain 6] and *MYL2* [myosin light chain 2]) (Figure 4D). These data suggest that carfilzomib increases contractile dysfunction after treatment.

## Carfilzomib Treatment Reduced Traction Forces and Caused Structural Disorganization

To further examine the carfilzomib-induced alteration in contraction, we used a DNA duplex TGT probe<sup>29</sup>

to measure integrin-mediated traction forces in single cardiomyocytes. The TGT probe was modified with a fibronectin mimetic ligand (cyclic-RGD [the tripeptide consists of arginine, glycine, and aspartate]), fluorophore (Cy3B), and quencher. When cell integrins bind to the RGD ligand and transmit a threshold magnitude of tension greater than the probe's tension tolerance (56 pN), the duplex mechanically denatures, and the fluorophore separates from the quencher. Because the biotin-anchored nucleic acid is also fluorescently tagged, shearing of the top strand leads to  $\approx 20$ -fold enhancement in fluorescence. Moreover, the fluorescence signal is directly proportional to the number of probes that experiences a threshold force exceeding 56 pN; therefore, the fluorescence signal provides a quantitative readout of integrin traction forces (Figure 5A). 3D hiPSC-CMs were treated with carfilzomib for 1 day, dissociated, and then reseeded onto the glass surface with the TGT probe. We then quantified the fluorescence signal of single cardiomyocytes upon plating to monitor the traction forces of spontaneously contracting cardiomyocytes. As shown in Figure 5B and 5C, the traction forces of hiPSC-CMs decreased in cultures treated with carfilzomib at 0.01, 0.1, 1, and 10  $\mu\text{mol/L}$  or doxorubicin compared with DMSO-treated cells. Thus, carfilzomib reduced integrin-mediated traction forces. To evaluate if structural changes were accompanied with the alteration in contraction induced by carfilzomib treatment, we measured the cell structure of hiPSC-CMs after carfilzomib treatment by immunocytochemistry of  $\alpha$ -actinin, a protein expressed in z-lines of cardiomyocytes. Cells treated with carfilzomib at 1 and 10  $\mu\text{mol/L}$  lacked clear z-lines, whereas the DMSO-treated cells and cells treated with carfilzomib at 0.01 and 0.1  $\mu\text{mol/L}$  had clear z-lines (Figure 6A). We also quantified cell size and shape along with sarcomere length to identify the link between the shape and contraction. Cells treated with higher concentrations of carfilzomib (1 and 10  $\mu\text{mol/L}$ ) showed decreased cell area compared with DMSO-treated cells; these cells also had irregular peripheral borders resulting in an increased circularity (Figure 6B). In addition, cells treated with carfilzomib at 0.01 and 0.1  $\mu\text{mol/L}$  or doxorubicin had shorter z-line length and sarcomere length compared with DMSO-treated cells (Figure 6B). These results indicate that carfilzomib treatment can induce significant structural alteration parallel with contractility dysfunction.

## Transcriptomic and Proteomic Analyses Revealed That Carfilzomib Dysregulated Genes Related to Stress Response, Extracellular Matrix, and Contractility

To further elucidate the mechanism of carfilzomib-induced alteration in contractility, we compared global

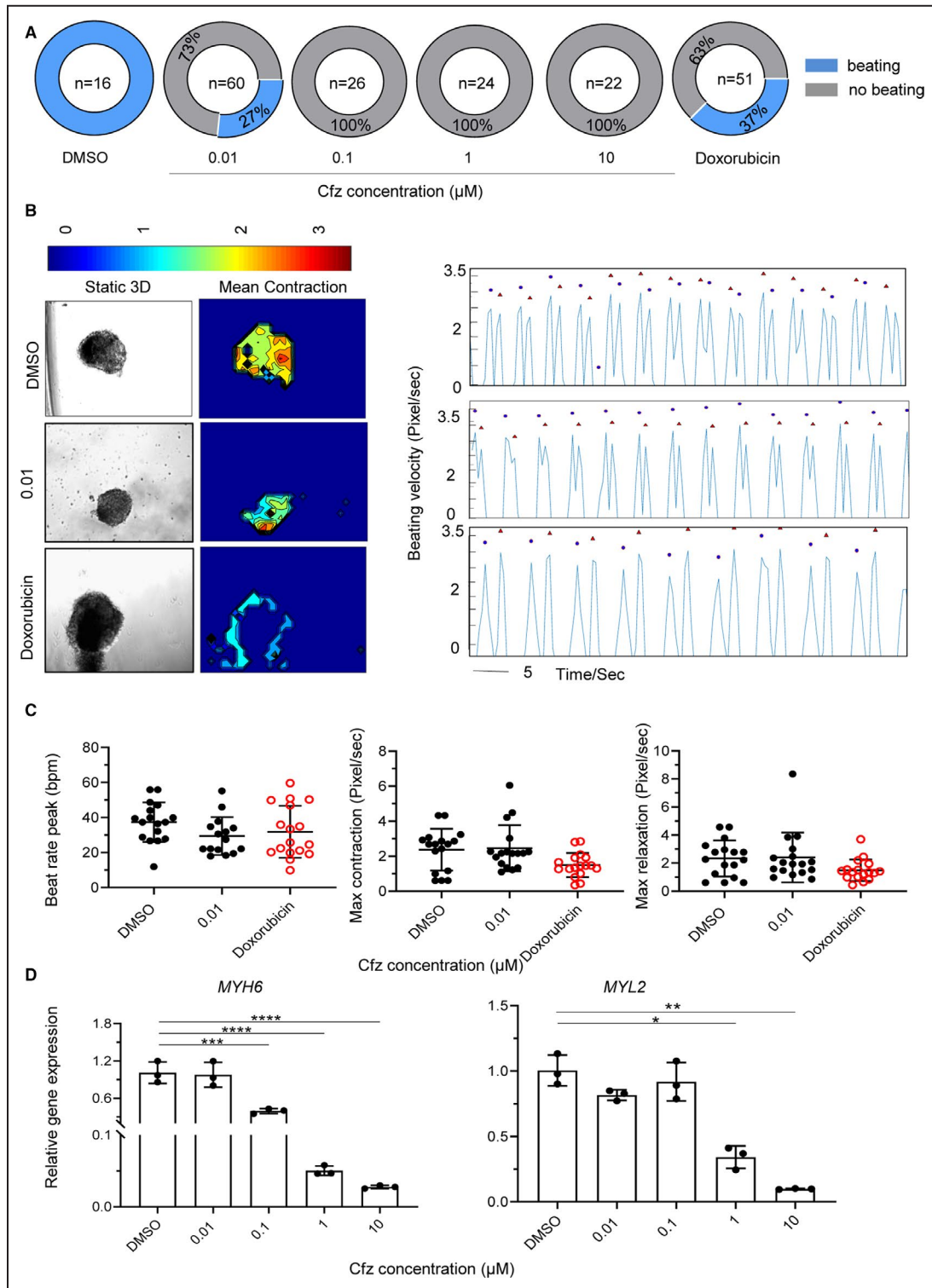


**Figure 4. Czf treatment induced contractility dysfunction in 3-dimensional (3D) human induced pluripotent stem cell-derived cardiomyocytes (hiPSC-CMs).**

**A**, Pie chart representing proportions of spheroids with or without beating arrest 24 hours after Czf treatment (n=16–60 cardiac spheroids). **B**, Contractility of static 3D hiPSC-CMs was video recorded and analyzed using MATLAB. Representative heat maps and graphs of averaged magnitude of beating speed over time in Czf-treated hiPSC-CMs. Red cycles and blue triangles represent contraction and relaxation, respectively. Note: hiPSC-CMs stopped beating following 24 hours of treatment of Czf at 0.1, 1, and 10 μmol/L. **C**, Quantification of contraction, relaxation, and beating rate among groups (n=14–17 cardiac spheroids). **D**, Expression of genes encoding contractile proteins *MYH6* (myosin heavy chain 6) and *MYL2* (myosin light chain 2) detected by quantitative reverse transcription–polymerase chain reaction (n=3 cultures). Czf indicates carfilzomib; and DMSO, dimethyl sulfoxide.



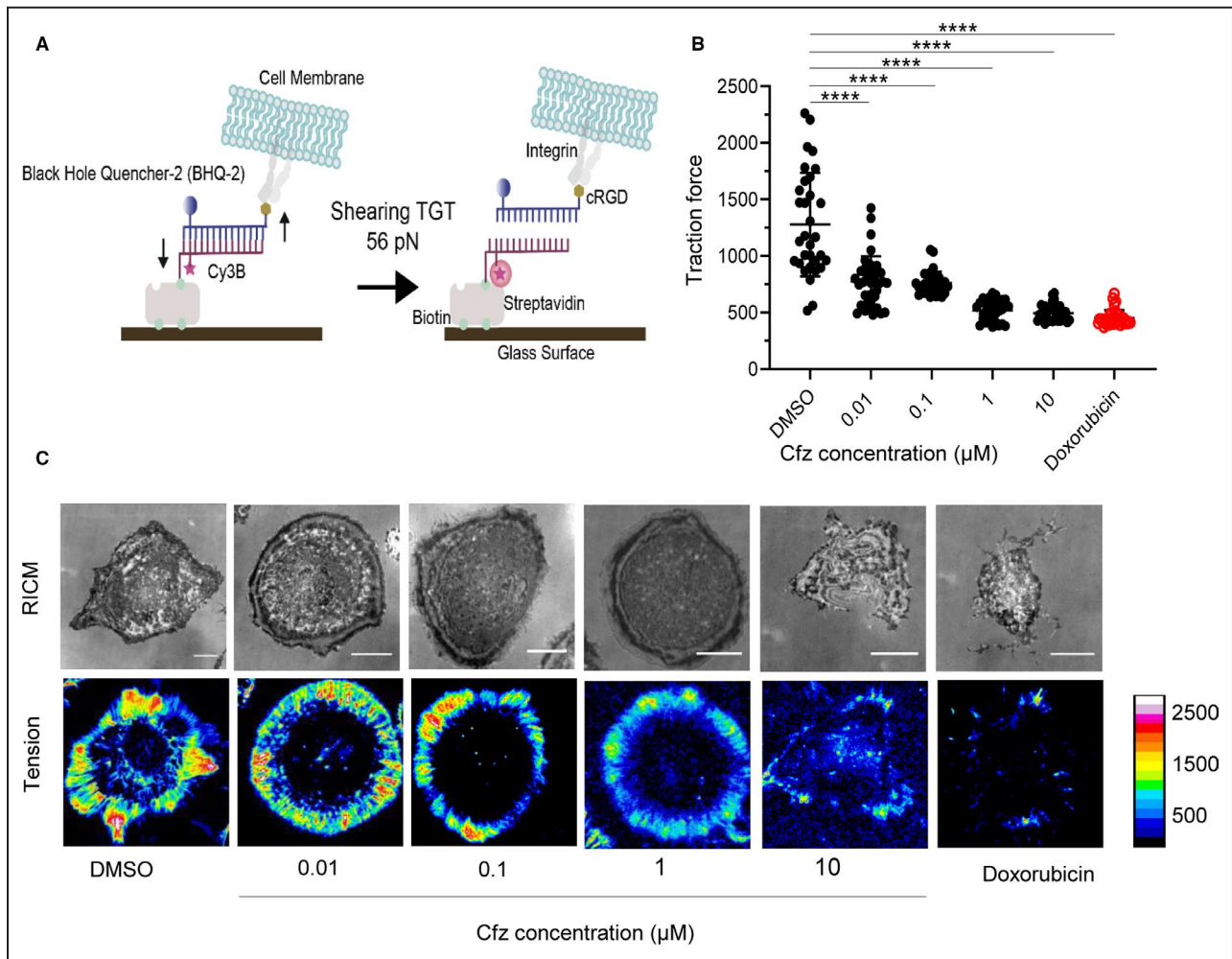


**Figure 5. Czf treatment reduced the traction forces of human induced pluripotent stem cell-derived cardiomyocytes (hiPSC-CMs).**

For quantification of molecular traction forces of spontaneously contracting cardiomyocytes, hiPSC-CMs were treated for 1 day with Czf and reseeded on the glass bottom microplates coated with the DNA probes through biotin streptavidin conjugation. **A**, Illustrative model of traction force measurement principle. The probes were decorated with peptide mimic (cRGDfk) of fibronectin, a fluorophore (Cy3B), and quencher (BHQ-2). Fluorescence intensity of the probes on the surface increases upon rupturing of the probes when cells contract and apply a force to the probes greater than the force tolerance of around 56 pN. **B**, Summary of traction force measurement in hiPSC-CMs treated with Czf vs DMSO (n=20–30 cells). \*\*\*\*P<0.0001. **C**, Representative traction force microscopy of hiPSC-CMs after Czf treatment. Scale bar=12 μm. Czf indicates carfilzomib; DMSO, dimethyl sulfoxide; pN, pico newton; RICM, reflection interference contrast microscopy; and TGT, tension gauge tether.

gene expression profile of hiPSC-CMs treated with carfilzomib at 1 μmol/L for 24 hours with DMSO-treated cells. RNA-seq analysis identified 5027 genes that were differentially expressed based on absolute log<sub>2</sub> (fold change) >1 and adjusted P<0.05. Compared with DMSO-treated cells, 1913 genes were upregulated, whereas 3114 genes were downregulated in carfilzomib-treated cells (Figure 7A). For example, carfilzomib induced downregulation of genes involved in cardiac muscle contraction (eg, *ACTA2* [actin alpha-2, smooth muscle]) and integrin complex (eg, *ITGA11* [integrin subunit alpha 11]). In addition, genes related to heat shock stress were upregulated, including *HSPA1B* (heat shock protein family A member 1B), *HSPA6* (heat

shock protein family A member 60), *HSPH1* (heat shock protein family H member 1), and *BAG3* (BAG cochaperone 3), which participate in cellular response to stress, cell death, and apoptosis.

We also performed analysis of GO terms using the differentially expressed genes. GO terms related to oxidative stress, heat shock proteins (HSPs) and proteasomal protein catabolic process were upregulated, and GO terms related to extracellular matrix (ECM) and cardiac contraction were downregulated (Figure 7B, Table 2). In line with carfilzomib-mediated mitochondrial oxidative stress, carfilzomib induced upregulation of GO terms including response to oxidative stress, ROS metabolic process, response to

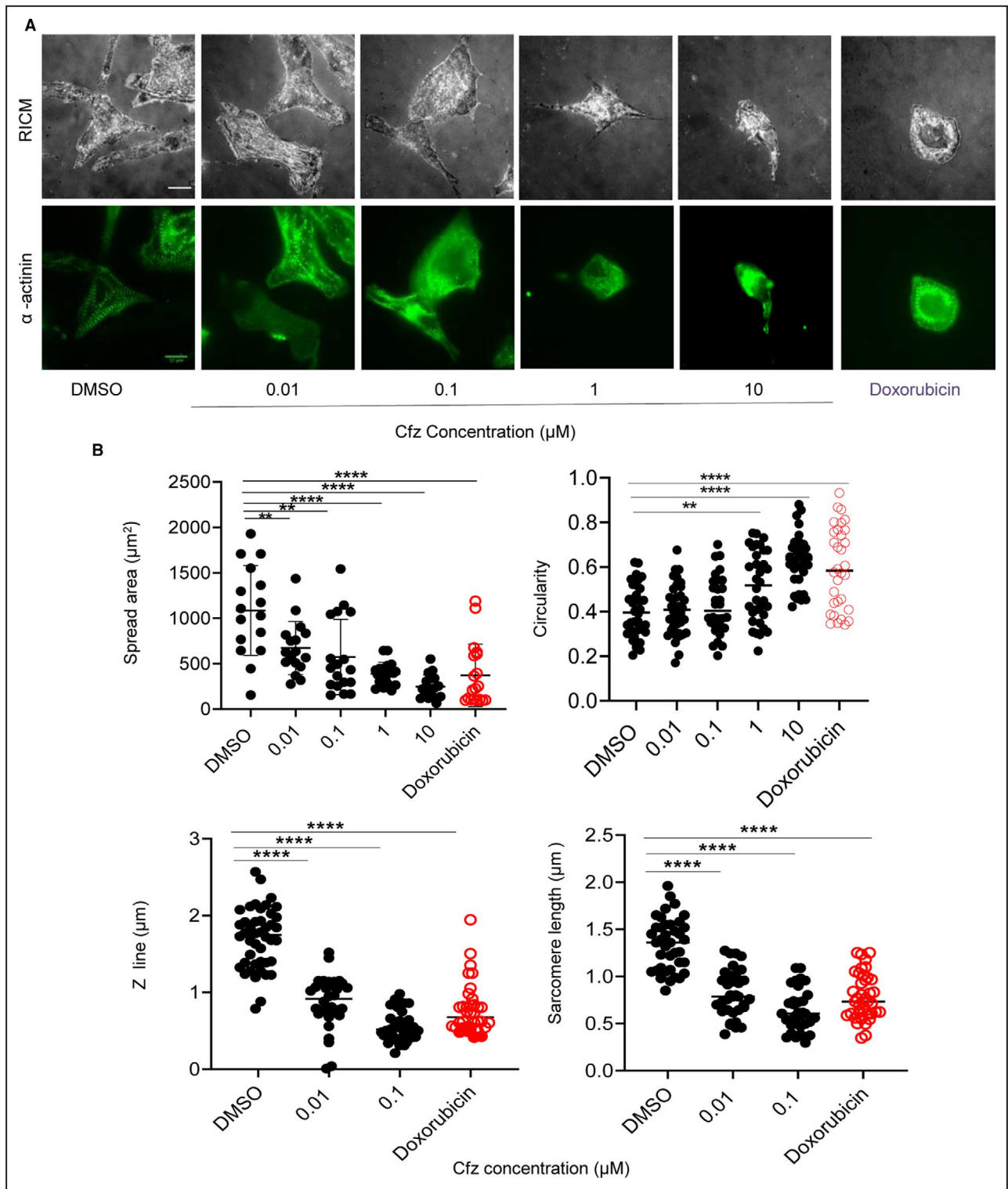


**Figure 6.** Czf treatment led to structural alterations in human induced pluripotent stem cell-derived cardiomyocytes (hiPSC-CMs).

hiPSC-CMs were treated with Czf for 24 hours, fixed, and stained with antibodies against  $\alpha$ -actinin. Cells were imaged using fluorescence microscopy and quantitatively analyzed. **A**, Representative RICM and fluorescence images of hiPSC-CMs treated with Czf. Scale bar=12  $\mu\text{m}$ . **B**, Summary of structural parameters of hiPSC-CMs after Czf treatment (n=20–30 cells). \*\* $P$ <0.01; \*\*\*\* $P$ <0.0001. Note that Czf treatment significantly decreased the spread area, z-line length, and sarcomere length and increased circularity. Cells treated with Czf at 1 and 10  $\mu\text{mol/L}$  did not show clear striation and z lines. Czf indicates carfilzomib; DMSO, dimethyl sulfoxide; and RICM, reflection interference contrast microscopy.

temperature stimulus, and cellular response to heat. In contrast, carfilzomib induced downregulation of GO terms of extracellular structure organization, extracellular matrix, actin binding, muscle system process, actin cytoskeleton, transmembrane receptor protein serine/threonine kinase signaling pathway, ECM structural constituent, contractile fiber, response to calcium ion, cardiac muscle contraction, and integrin binding and pathway-restricted Smad protein phosphorylation.

The top downregulated genes based on fold change included those involved in integrin and ECM (*ITGA11*, *MEGF6* [multiple EGF like domains 6], *FJX1* [four-jointed box kinase 1], *MFAP4* [microfibril associated protein 4], *CCDC80* [coiled-coil domain containing 80], and *FNDC10* [fibronectin type III domain containing 10]), mitochondria (*SLIT3* [slit guidance ligand 3], *DUT* [deoxyurine triphosphatase], *PCK2* [phosphoenolpyruvate carboxykinase 2, mitochondrial], and *ATP6V0E2* [ATPase H<sup>+</sup> transporting V0 subunit E2]) and muscle contraction/tight junction (*ACTA2* [actin alpha 2, smooth muscle] and *SYNPO* [Synaptopodin]) (Table 3). The top upregulated genes included genes involved in response to oxidative stress, heat stress, and ROS metabolic process, including *HSPA1B*, *HSPA1A* (heat shock protein family H member 1), *DNAJA1* (DnaJ heat shock protein family member A1), *BAG3*, and *HSP90AB1* (heat shock protein 90 alpha family class B member 1) (Table 4). Additionally, carfilzomib upregulated genes involved in mitogen-activated protein kinase-mediated signaling cascade (*MAP2K3*) and downregulated genes involved in Smad pathway (*BMP10* and *BMP7*) (Figure 7B). Carfilzomib also altered the expression of genes associated with ECM-receptor interaction, cell cycle, protein digestion and absorption, dilated cardiomyopathy, and hypertrophic cardiomyopathy (Figure 7C).

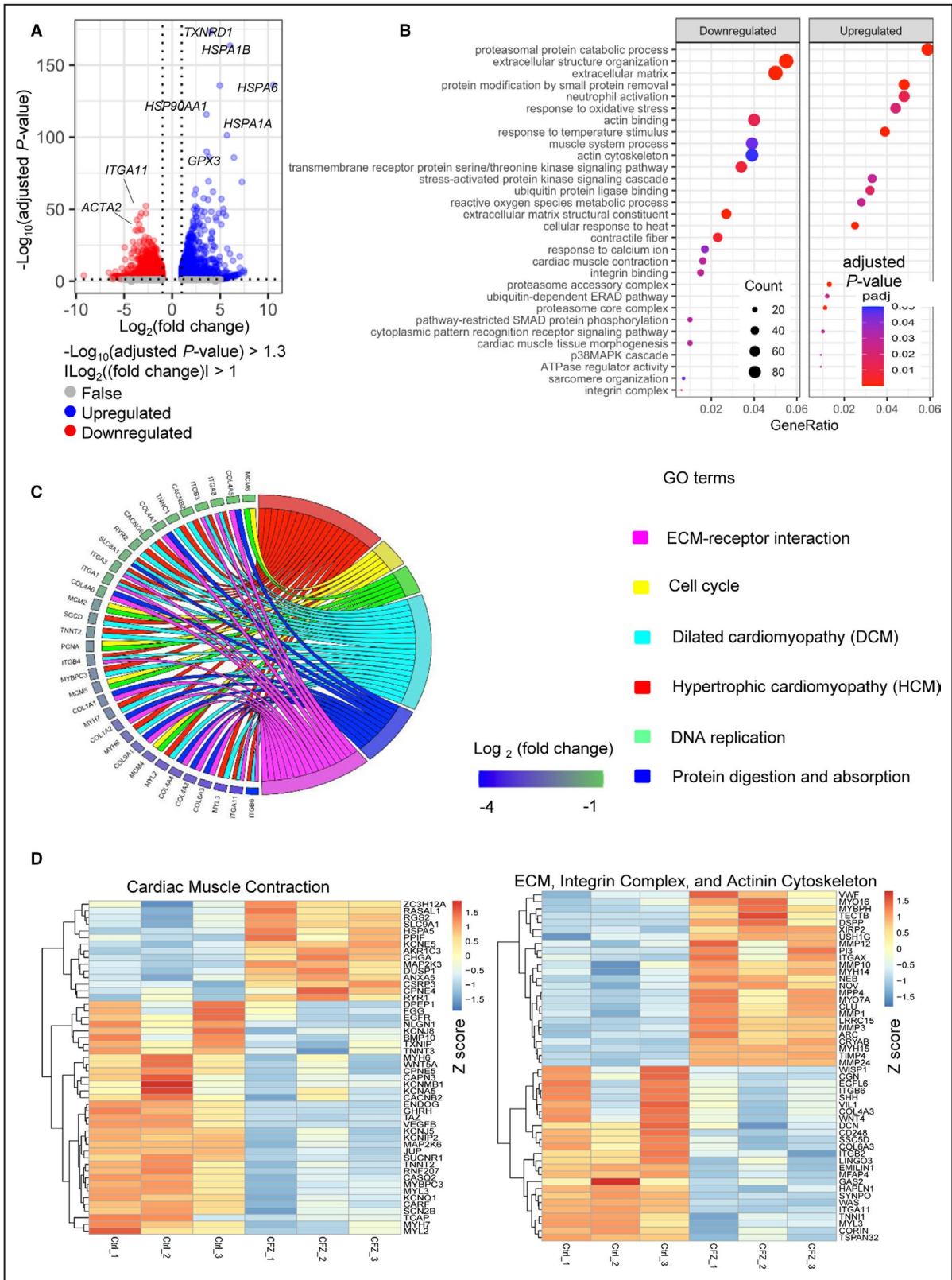
We further analyzed the differentially expressed genes based on Z scores. As shown in the heatmap (Figure 7D), the expression of genes related to cardiac muscle contraction was dramatically downregulated in carfilzomib-treated cells compared with DMSO-treated cells. These genes included response to calcium ion (*TNNT2* [troponin T2, cardiac type], *EEF2K* [eukaryotic elongation factor 2 kinase], *CARF* [calcium responsive transcription factor], *MYL3* [myosin light chain 3], *MAP2K6* [mitogen-activated protein kinase 6], *MYB* [MYB proto-oncogene, transcription factor], *KCNJ5* [potassium inwardly rectifying channel subfamily J member 5], *KCNQ1* [potassium voltage-gated channel subfamily Q member 1], *TNNT2*, *MYH7* [myosin heavy chain 7], *RYR2*, and *CASQ2*), calcium responsive proteins (*RYR2*, *SLC25A12* [solute carrier family 25 member 12], *CASQ2*, and *KCNMB1*), and contractile proteins (*SYNPO* [synaptopodin], *ACTA2*, *FLNC* [filamin C], *BMF* [Bcl2 modifying factor], *MYL3*,

*MYO1D* [myosin ID], *ZNF185* [zinc finger protein 185 with LIM domain], *TNNI1* [troponin I1, slow skeletal type], *TNNT3* [troponin T3, fast skeletal type], *MYL2*, *MYL5* [myosin light chain 5], *MYLK* [myosin light chain kinase], *MYO5C* [myosin VC], *MYO15B* [myosin XVb], *MYH6*, and *MYL7* [myosin light chain 7]). In addition, carfilzomib-dysregulated genes were involved in ECM, integrin complex, and actinin cytoskeleton. These genes included *ITGA11*, *SYNPO*, *SLC6A4* [solute carrier family 6 member 4], *CASQ2*, *TNNI1*, and *MYL3* (Figure 7D).

To examine the effect of carfilzomib at the protein level, we performed quantitative proteomic analysis on both the cell supernatant and cell lysate of hiPSC-CMs treated with carfilzomib at 1 μmol/L versus DMSO for 24 hours. Out of the 4060 proteins quantified in the cell lysate, 183 proteins were upregulated, and 39 proteins were downregulated (Figure 8A). Out of the 298 proteins detected in the cell supernatant, 6 proteins were upregulated, and 18 proteins were downregulated after carfilzomib treatment ( $P < 0.05$ , absolute fold change  $> 1.3$ ) (Figure 8B). The downregulated proteins in the cell lysate included ANXA6 (annexin A6, a calcium-dependent membrane and phospholipid binding protein), SPTN1 (spectrin alpha, non-erythrocytic 1, a filamentous cytoskeletal protein highly expressed in cardiac muscle at z-disc), and TPM1 (tropomyosin 1, a protein that forms a complex with troponin T and regulates actin-myosin interaction in response to intracellular Ca<sup>2+</sup> concentration).

As shown in Figure 8A, carfilzomib treatment reduced the expression of proteins in the cells associated with metabolic process, including pyruvate kinase M2 (PKM2), which is involved in glycolysis and regulates cardiomyocyte cell cycle, and protein kinase cAMP-activated catalytic subunit alpha (PRKACA), which is the catalytic subunit α of protein kinase A that contributes to the control of glucose metabolism and cell division. The downregulated proteins were associated with GO terms of metabolic process (PRKACA [protein kinase cAMP-activated catalytic subunit alpha], SDHAF2 [succinate dehydrogenase complex assembly factor 2], PGAM2 [phosphoglycerate mutase 2], GOT1 [glutamic-oxaloacetic transaminase 1], IMPA1 [inositol monophosphatase 1], CLEC16A [C-type lectin domain containing 16A], and ATM [ATM serine/threonine kinase]), mitochondrion organization (SDHFA2, GGCT [gamma-glutamylcyclotransferase], and MICOS13 [mitochondrial contact site and cristae organizing system subunit 13]), striated muscle contraction (PRKACA, GSTM2 [glutathione S-transferase mu 2], PGAM2, TPM1, and RCSD1 [RCSD domain containing 1]), oxidation reduction (FDX1 [ferredoxin 1], HADH [hydroxyacyl-CoA dehydrogenase], IDH3G [isocitrate dehydrogenase (NAD(+)) 3 non-catalytic subunit gamma]), PGAM2, PKM [pyruvate kinase M1/2],





TPI1 [triosephosphate isomerase 1], and SDHAF2), and muscle system process (ANXA [annexin A], GSTM2 [glutathione S-transferase mu 2], PGAM2, PRKACA, TPM1, and RCSD1) (Figure 9A, Table 5).

The enriched GO terms of upregulated proteins in the cells included cellular response to stress, ubiquitin-dependent protein catabolic process, protein folding, regulation of cellular response to heat, cell death, and



**Figure 7. Cfz treatment altered global gene expression in human induced pluripotent stem cell-derived cardiomyocytes (hiPSC-CMs).**

Gene expression profiling of hiPSC-CMs after treatment with 1  $\mu\text{mol/L}$  Cfz for 24 hours was analyzed by RNA sequencing ( $n=3$  cultures). DEGs in cells after Cfz were compared with those in the cells treated with DMSO. Volcano plot representing 3114 downregulated genes and 1913 upregulated genes are depicted in the red and blue dots, respectively. DEGs between the 2 groups were defined based on adjusted  $P < 0.05$  and the absolute value of  $\log_2$  (fold change)  $\geq 1$ . **B**, Bubble plots representing enrichment analysis of DEGs using GO enrichment analysis. **C**, Chord diagram of relationship between selected GO terms and relevant DEGs. Each GO term is shown on the right, and genes contributing to these enrichments are presented on the left. Colored squares next to each gene indicate  $\log_2$  (fold change) from the highest to the lowest level. **D**, Heatmap of DEGs associated with cardiac muscle contraction (left) and ECM, integrin complex, and actinin cytoskeleton (right). Red color indicated relatively high expression and blue color indicated relatively low expression based on Z score. ACTA2 indicates actin alpha 2, smooth muscle; AKR1C3, aldo-keto reductase family 1 member C3; ANXA5, annexin A5; ARC, activity regulated cytoskeleton associated protein; BMP10, bone morphogenetic protein 10; CACNB2, calcium voltage-gated channel auxiliary subunit beta 2; CACNG6, calcium voltage-gated channel auxiliary subunit gamma 6; CAPN3, calpain 3; CARF, calcium responsive transcription factor; CASQ2, calsequestrin 2; CCDC80, coiled-coil domain containing 80; CD248, CD248 molecule; Cfz, carfilzomib; CGN, cingulin; CHGA, chromogranin A; CLU, clusterin; COL1A1, collagen type I alpha 1 chain; COL1A2, collagen type I alpha 2 chain; COL3A1, collagen type III alpha 1 chain; COL4A1, collagen type IV alpha 1 chain; COL4A3, collagen type IV alpha 3 chain; COL4A4, collagen type IV alpha 4 chain; COL4A5, collagen type IV alpha 5 chain; COL4A6, collagen type IV alpha 6 chain; COL6A3, collagen type VI alpha 3 chain; COL9A1, collagen type IX alpha 1 chain; CORIN, corin, serine peptidase; CPNE4, copine 4; CPNE5, copine 5; CRYAB, crystallin alpha B; CSRP3, cysteine and glycine rich protein 3; DCN, decorin; DEGs, differentially expressed genes; DMSO, dimethyl sulfoxide; DPEP1, dipeptidase 1; DUSP1, dual specificity phosphatase 1; ECM, extracellular matrix; EGFL6, EGF like domain multiple 6; EGFR, epidermal growth factor receptor; EMILIN1, elastin microfibril interfacer 1; ENDOG, endonuclease G; FERMT3, FERM domain containing kindlin 3; FLNC, filamin C; FN1, fibronectin 1; GAA, alpha glucosidase; GAS2, growth arrest specific 2; GO, gene ontology; GPX3, glutathione peroxidase 3; HAPLN1, hyaluronan and proteoglycan link protein 1; HMGCR, 3-hydroxy-3-methylglutaryl-CoA reductase; HSP90AA1, heat shock protein 90 alpha family class A member 1; HSPA1A, heat shock protein family A; HSPA1B, heat shock protein family A; HSPA5, heat shock protein family A; HSPA6, heat shock protein family A; ITGA1, integrin subunit alpha 1; ITGA11, integrin subunit alpha 11; ITGA3, integrin subunit alpha 3; ITGA8, integrin subunit alpha 8; ITGAX, integrin subunit alpha X; ITGB3, integrin subunit beta 3; ITGB4, integrin subunit beta 4; ITGB6, integrin subunit beta 6; JUP, junction plakoglobin; KCNA5, potassium voltage-gated channel subfamily A member 5; KCNE5, potassium voltage-gated channel subfamily E regulatory subunit 5; KCNIP2, potassium voltage-gated channel interacting protein 2; KCNJ5, potassium inwardly rectifying channel subfamily J member 5; KCNJ8, potassium inwardly rectifying channel subfamily J member 8; KCNMB1, potassium calcium-activated channel subfamily M regulatory beta subunit 1; KCNQ1, potassium voltage-gated channel subfamily Q member 1; LRRC15, leucine rich repeat containing 15; MAFG, MAF bZIP transcription factor G; MAP2K3, mitogen-activated protein kinase kinase 3; MAP2K6, mitogen-activated protein kinase kinase 6; MCM2, minichromosome maintenance complex component 2; MCM4, minichromosome maintenance complex component 4; MCM5, minichromosome maintenance complex component 5; MCM6, minichromosome maintenance complex component 6; MFAP4, microfibril associated protein 4; MMP1, matrix metalloproteinase 1; MMP10, matrix metalloproteinase 10; MMP12, matrix metalloproteinase 12; MMP24, matrix metalloproteinase 24; MMP3, matrix metalloproteinase 3; MPP4, membrane palmitoylated protein 4; MSN, moesin; MUC4, mucin 4, cell surface associated; MYBPC3, myosin binding protein C3; MYBPH, myosin binding protein H; MYH14, myosin heavy chain 14; MYH15, myosin heavy chain 15; MYH6, myosin heavy chain 6; MYH7, myosin heavy chain 7; MYL2, myosin light chain 2; MYL3, myosin light chain 3; MYO16, myosin XVI; MYO7A, myosin VIIA; NEB, nebulin; NLGN1, neuroligin 1; NTN1, netrin 1; PCNA, proliferating cell nuclear antigen; PHOSPHO1, phosphoethanolamine/phosphocholine phosphatase 1; PHPT1, phosphohistidine phosphatase 1; PKM, pyruvate kinase M1/2; POSTN, periostin; PPIF, peptidylprolyl isomerase F; RASAL1, RAS protein activator like 1; REL2, RELT like 2; RGS2, regulator of G protein signaling 2; RND3, Rho family GTPase 3; RNF207, ring finger protein 207; RYR1, ryanodine receptor 1; RYR2, ryanodine receptor 2; SCN2B, sodium voltage-gated channel beta subunit 2; SCN5A, sodium voltage-gated channel alpha subunit 5; SERPINE1, serpin family E member 1; SGCD, sarcoglycan delta; SHH, sonic hedgehog signaling molecule; SLC8A1, solute carrier family 8 member A1; SLC9A1, solute carrier family 9 member A1; SOD1, superoxide dismutase 1; SSC5D, scavenger receptor cysteine rich family member with 5 domains; ST13, ST13 Hsp70 interacting protein; SUCNR1, succinate receptor 1; SYNPO, synaptopodin; TAFAZZIN, tafazzin, phospholipid-lysophospholipid transacylase; TCAP, titin-cap; TIMP4, TIMP metalloproteinase inhibitor 4; TNNC1, troponin C1, slow skeletal and cardiac type; TNNI1, troponin I1, slow skeletal type; TNNT2, troponin T2, cardiac type; TNNT3, troponin T3, fast skeletal type; TSPAN32, tetraspanin 32; TXNIP, thioredoxin interacting protein; TXNRD1, thioredoxin reductase 1; VCP, valosin containing protein; VEGFB, vascular endothelial growth factor B; VIL1, villin 1; WAS, WASP actin nucleation promoting factor; WNT5A, Wnt family member 5A; XIRP2, xin actin binding repeat containing 2; and ZC3H12A, zinc finger CCCH-type containing 12A.

stress-activated mitogen-activated protein kinase cascade (Figure 9B). In addition, proteins associated with oxidative stress, autophagy, apoptosis and cell cycle were upregulated in the cells, including MAFG (MAF bZIP transcription factor G, a transcription factor that is induced following oxidative stress), ATG101 (autophagy related 101, an essential protein for the initiation of autophagy), RND3 (Rho family GTPase 3, a member of the small Rho GTPase family that regulates apoptosis), and CDKN1A (cyclin dependent kinase inhibitor 1, Figure 8A, Table 6).

The downregulated proteins in the secretome included POSTN (periostin), C1S (complement C1s), THBS1 (thrombospondin 1), and COL3A1 (collagen type III alpha 1 chain) (Figure 8B, Table 7). THBS1 is an adhesive glycoprotein that mediates cell-to-cell and cell-to-ECM interactions, COL3A1 provides instructions for making type III collagen that strengthens and supports cardiac tissue, and POSTN is a ligand for integrins providing the support for cell adhesion. The downregulated proteins in secretome are associated with GO terms including extracellular

**Table 2. Top Downregulated GO Terms Based on DEGs**

GO term	Category	No. of genes	GO term ID	Adjusted P value	Enrichment
Extracellular matrix	Biological process	106	GO:0031012	1.24E-17	3.2
Extracellular structure organization	Cellular component	108	GO:0043062	2.02E-12	3
Extracellular matrix structural constituent	Morphological function	54	GO:0005201	1.37E-10	3.6
Contractile fiber	Biological process	49	GO:0043292	0.006207	2.3
Transmembrane receptor protein serine/threonine kinase signaling pathway	Cellular component	68	GO:0007178	0.007959	2.1
Integrin complex	Morphological function	12	GO:0008305	0.010804	3.4
Actin binding	Morphological function	79	GO:0003779	0.012514	2
Integrin binding	Biological process	29	GO:0005178	0.027535	2.5
Pathway-restricted Smad protein phosphorylation	Biological process	19	GO:0060389	0.028713	3.1
Cardiac muscle contraction	Biological process	31	GO:0060048	0.028713	2.7
Cardiac muscle tissue morphogenesis	Biological process	20	GO:0055008	0.028713	3.2
Response to calcium ion	Biological process	34	GO:0051592	0.03831	2.4
Muscle system process	Biological process	77	GO:0003012	0.044283	1.8
Sarcomere organization	Cellular component	14	GO:0045214	0.046017	3.4
Actin cytoskeleton	Cellular component	83	GO:0015629	0.048669	1.7

DEGs indicates differentially expressed genes; and GO, gene ontology.

matrix organization, cell-matrix adhesion, and cell motility (Figure 9C) and *Kyoto Encyclopedia of Genes and Genomes* pathways including tight junction and DNA replication (Table 8). In addition, upregulation of HSPA1A was observed in both the cells and the secretome (Figure 8A and 8B, Table 7).

Comparison of the proteomic and transcriptomic data revealed a set of overlapping genes and proteins that were differentially expressed in response to carfilzomib treatment (Figure 8C and 8D). We performed additional GO-term analysis using these overlapping genes and proteins (Figure 8E, Table 9). The enriched GO terms included response to heat, HSP binding, and ATPase regulator activity (Figure 8E). Several pathways were upregulated, including apoptotic signaling (*ATF3* [activating transcription factor 3], *CDKN1A*, *DNAJA1*, *HSPA1A*, *SERPINE1* [serpin family E member 1], *BAG3*, and *USP47* [ubiquitin specific peptidase 47]), stress-activated mitogen-activated protein kinase cascade (*CRYAB*, *HMGCR* [3-hydroxy-3-methylglutaryl-CoA reductase], *DNAJA1*, *SKP1* [S-Phase Kinase Associated Protein 1], and *UBB* [ubiquitin B]) and ATPase activity (*DNAJA1*, *DNAJB1* [DnaJ heat shock protein family (Hsp40) member B1], *BAG3*, *HSPH1*, and *DNAJB4* [DnaJ heat shock protein family (Hsp40) member B4]) (Table 9). We note that RNA-seq was analyzed using hiPSC-CMs derived from the SCVI-273 line, and proteomics analysis was performed using hiPSC-CMs derived from IMR-90 hiPSCs. The consistency in the alterations in the expression of these overlapping genes and proteins in 2 cell lines suggests that the

observed alterations induced by carfilzomib treatment are independent of the cell lines used.

In addition, carfilzomib treatment upregulated several ubiquitin-related proteins. As detected by RNA-seq, ubiquitin C was among the top 20 upregulated proteins (Table 4). Proteomic analysis of cell lysates also revealed that several ubiquitin-related proteins were upregulated, including negative regulator of ubiquitin like proteins 1, praja ring finger ubiquitin ligase 2, ubiquitin specific peptidase 33, and ubiquitin B (Table 6). GO-term analysis of differentially expressed proteins identified ubiquitin protein ligase binding (n=44) and ubiquitin-dependent ERAD (endoplasmic reticulum-associated degradation) pathway (n=16). These changes may indicate the direct effect of carfilzomib on the ubiquitin-proteasome pathway.

Taken together, the transcriptomic and proteomic analyses of hiPSC-CMs indicate that downregulation of contractile-related genes/proteins, and ECM and integrin-related genes/proteins together with upregulation of HSPs and stress-activated pathways were associated with cardiac-toxic effects of carfilzomib treatment.

## DISCUSSION

Using molecular tension sensors to quantify cellular traction forces in combination with high-throughput imaging, functional assessments, and transcriptomic and proteomic analyses, we investigated mechanisms of earlier cellular and molecular events associated

**Table 3. Top Downregulated DEGs**

Gene ID	Gene symbol	Description of full name	Adjusted P value	Log <sub>2</sub> , fold change
ENSG00000177943	<i>MAMDC4</i>	MAM domain containing 4	4.94E-56	-9.199087572
ENSG00000171992	<i>SYNPO</i>	Synaptopodin	8.84E-51	-6.60093912
ENSG00000104738	<i>MCM4</i>	Minichromosome maintenance complex component 4	1.11E-50	-6.261530975
ENSG00000137809	<i>ITGA11</i>	Integrin subunit alpha 11	2.58E-48	-6.196870403
ENSG00000184347	<i>SLIT3</i>	Slit guance ligand 3	5.13E-46	-6.157781163
ENSG00000156427	<i>FGF18</i>	Fibroblast growth factor 18	6.14E-43	-6.150872209
ENSG00000185567	<i>AHNAK2</i>	AHNAK nucleoprotein 2	3.69E-39	-6.083552672
ENSG00000128951	<i>DUT</i>	Deoxyurine triphosphatase	7.18E-39	-6.012024116
ENSG00000225138	<i>None</i>	None	1.01E-38	-5.979760829
ENSG00000166482	<i>MFAP4</i>	Microfibril associated protein 4	2.35E-38	-5.973236912
ENSG00000107796	<i>ACTA2</i>	Actin alpha 2, smooth muscle	4.87E-34	-5.900336258
ENSG00000162591	<i>MEGF6</i>	Multiple EGF like domains 6	5.24E-33	-5.883525697
ENSG00000179431	<i>FJX1</i>	Four-jointed box kinase 1	1.35E-31	-5.691046545
ENSG00000157637	<i>SLC38A10</i>	Solute carrier family 38 member 10	2.21E-31	-5.669748257
ENSG00000171130	<i>ATP6V0E2</i>	ATPase H <sup>+</sup> transporting V0 subunit e2	8.55E-31	-5.627308177
ENSG00000129103	<i>SUMF2</i>	Sulfatase modifying factor 2	9.96E-31	-5.615074065
ENSG00000100889	<i>PCK2</i>	Phosphoenolpyruvate carboxykinase 2, mitochondrial	1.01E-30	-5.606701278
ENSG00000228594	<i>FNDC10</i>	Fibronectin type III domain containing 10	1.94E-30	-5.571960443
ENSG00000091986	<i>CCDC80</i>	Coiled-coil domain containing 80	6.85E-30	-5.561040949
ENSG00000100297	<i>MCM5</i>	Minichromosome maintenance complex component 5	2.30E-29	-5.547162364

DEGs indicates differentially expressed genes.

with alterations of contraction after carfilzomib treatment in hiPSC-CMs. Our results suggest a possible role of ECM and integrin-related genes in contractility

and traction force defects as an early response to carfilzomib treatment. We also identified increased mitochondrial oxidative stress, reduced mitochondrial

**Table 4. Top Upregulated DEGs**

Gene ID	Gene symbol	Description of full name	P value	Log <sub>2</sub> , fold change
ENSG00000198431	<i>TXNRD1</i>	(Thioredoxin reductase 1)	4.82E-178	4.006453
ENSG00000204388	<i>HSPA1B</i>	Heat shock protein family A (Hsp70) member 1B	3.04E-168	6.043998
ENSG00000173110	<i>HSPA6</i>	Heat shock protein family A (Hsp70) member 6	1.07E-140	10.52902
ENSG00000178381	<i>ZFAND2A</i>	Zinc finger AN1-type containing 2A	3.06E-140	4.963423
ENSG00000080824	<i>HSP90AA1</i>	Heat shock protein 90 alpha family class A member 1	4.45E-120	3.567891
ENSG00000204389	<i>HSPA1A</i>	Heat shock protein family H (Hsp110) member 1	1.35E-105	5.713138
ENSG00000120694	<i>HSPH1</i>	Heat shock protein family H (Hsp110) member 1	4.87E-94	3.593188
ENSG00000151929	<i>BAG3</i>	BAG cochaperone 3	2.72E-90	3.825662
ENSG00000187134	<i>AKR1C1</i>	Aldo-keto reductase family 1 member C1	7.03E-90	6.435566
ENSG00000211445	<i>GPX3</i>	Glutathione peroxidase 3	2.76E-73	3.792141
ENSG00000248713	<i>C4orf54</i>	Chromosome 4 open reading frame 54	7.41E-73	7.267963
ENSG00000096384	<i>HSP90AB1</i>	Heat shock protein 90 alpha family class B member 1	1.18E-67	2.472503
ENSG00000132002	<i>DNAJB1</i>	DnaJ heat shock protein family (Hsp40) member B1	4.49E-66	4.255973
ENSG0000013275	<i>PSMC4</i>	Proteasome 26S subunit, ATPase 4	3.71E-64	2.343216
ENSG00000150991	<i>UBC</i>	Ubiquitin C	1.83E-61	3.294192
ENSG00000272899	<i>ATP6V1FNB</i>	(ATP6V1F neighbor)	6.66E-61	5.123917
ENSG00000023909	<i>GCLM</i>	Glutamate-cysteine ligase modifier subunit	2.35E-60	3.747229
ENSG00000116161	<i>CACYBP</i>	Calcylin binding protein	7.54E-56	2.419254
ENSG00000197170	<i>PSMD12</i>	Proteasome 26S subunit, non-ATPase 12	1.96E-54	2.627123

DEGs indicates differentially expressed genes.

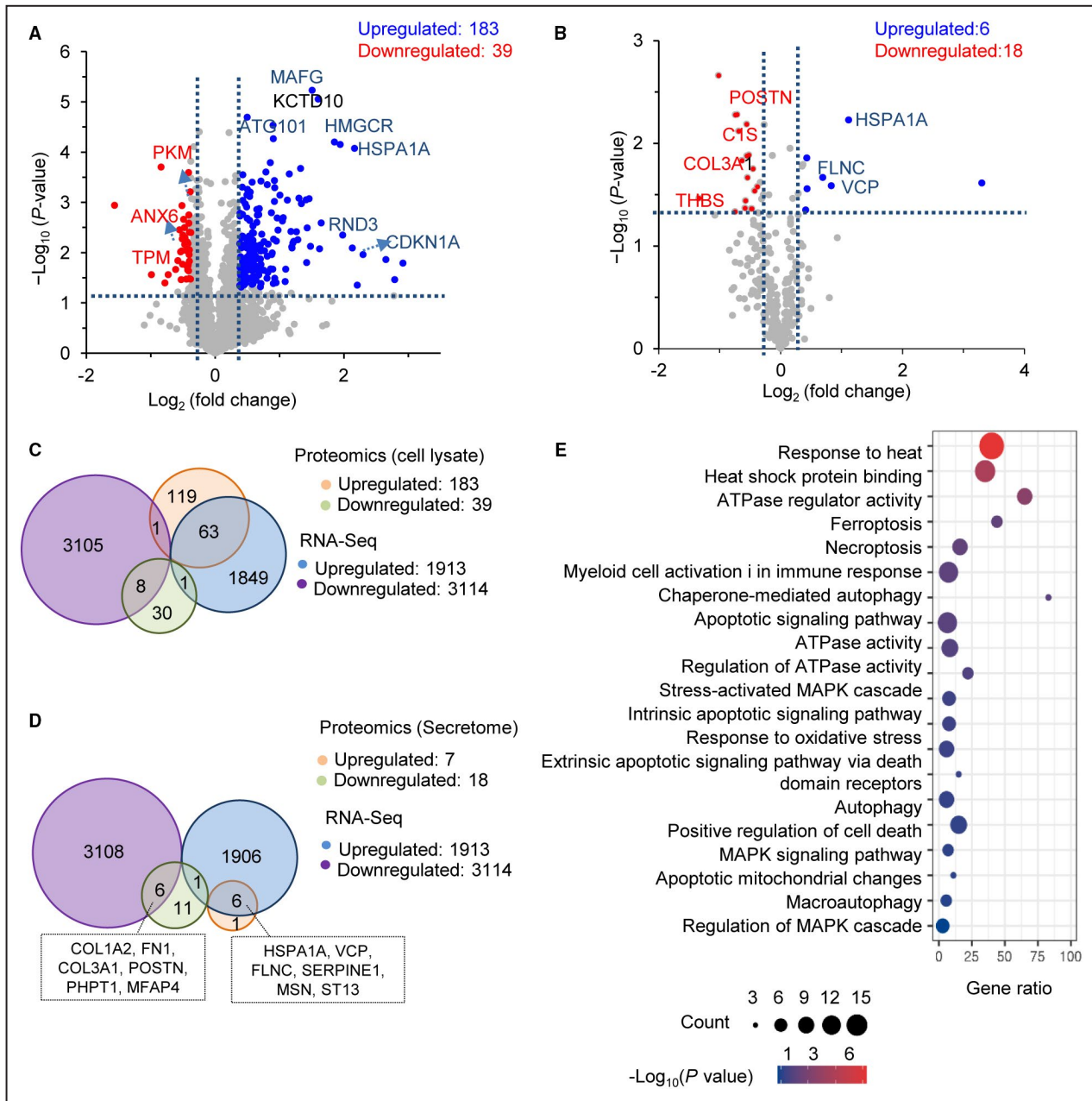


**Figure 8. Profiling of proteins after Cfz treatment by proteomics.**

DEPs were identified with abundance change by >1.3-fold (absolute  $\log_2$  [fold change] >0.38) compared with the DMSO-treated group (n=3 cultures). **A** and **B**, Volcano plot illustrating proteins in the cell lysate (right) and secreted proteins (left) with statistically significant abundance differences. Significantly upregulated proteins are marked in blue, and significantly downregulated proteins are in red. **C** and **D**, Venn diagram showing overlapping of DEGs and DEPs after Cfz treatment in the cell lysate and the secretome. **E**, Bubble plot represents selected GO terms based on overlapped DEGs and DEPs with significant upregulation. ANX6 indicates annexin 6; ATG101, autophagy related 101; CDKN1A, cyclin dependent kinase inhibitor 1A; Cfz, carfilzomib; C1S complement C1s; COL1A2, collagen type I alpha 2 chain; COL3A1, collagen type III alpha 1 chain; COL3A1, collagen type III alpha 1 chain; DEGs, differentially expressed genes; DEPs, differentially expressed proteins; DMSO, dimethyl sulfoxide; FLNC, filamin C; FN1, fibronectin 1; GO, gene ontology; HMGCR, 3-hydroxy-3-methylglutaryl-CoA reductase; HSPA1A, heat shock protein family A, Hsp70 member 1A; HSPA1A, heat shock protein family A, Hsp70 member 1A; HSPA1A, heat shock protein family A, Hsp70 member 1A; KCTD10, potassium channel tetramerization domain containing 10; MAFG, MAF bZIP transcription factor G; MFAP4, microfibril associated protein 4; MSN, moesin; Not Found; PHPT1, phosphohistidine phosphatase 1; PKM, pyruvate kinase M1/2; POSTN, periostin; RNA-seq, RNA sequencing; RND3, Rho family GTPase 3; SERPINE1, serpin family E member 1; ST13, ST13 Hsp70 interacting protein; TPM, tropomyosin; VCP, valosin containing protein; and VCP, valosin containing protein.

function, abnormal  $Ca^{2+}$  transients, and changes in the sarcomere structure and cell morphology that might impact the contractile potency and traction forces of

hiPSC-CMs after carfilzomib treatment. Transcriptomic and proteomic analyses highlighted an important role of the genes involved in ECM signaling including integrin



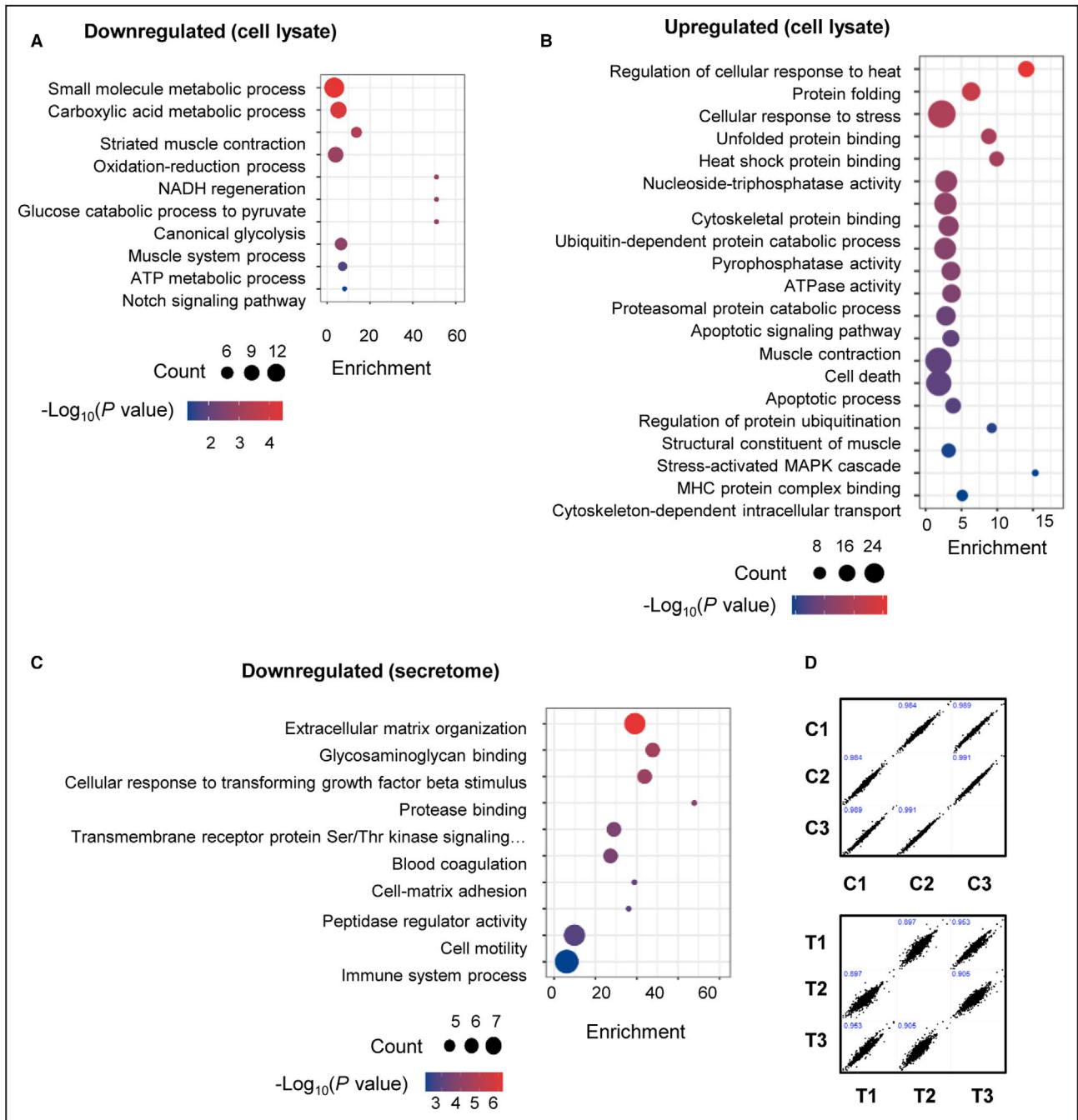


**Figure 9. Profiling of protein changes in response to Cfz treatment in human induced pluripotent stem cell-derived cardiomyocytes.**

**A** and **B**, GO-term enrichment of the downregulated and upregulated proteins in the cell lysate. **C**, GO-term enrichment of the downregulated secreted proteins. **D**, Pearson correlation of biological triplicate experiments of control group (C1–3) and Cfz-treated group (T1–3). Pearson correlation coefficient (*r*) values are depicted for each group. Cfz indicates carfilzomib; and GO, gene ontology.

and actin filaments. In parallel, our study revealed an increase in genes associated with stress response (eg, HSPs). These results suggest that cardiotoxicity can result from the cumulative response to both off-target and on-target effects of carfilzomib treatment.

Since the Food and Drug Administration’s approval of carfilzomib in 2012, there has been increasing

evidence surrounding carfilzomib-associated adverse cardiovascular events including cardiac arrest and cardiac arrhythmias.<sup>1,3,4,6</sup> Carfilzomib is also considered as an approved drug with repurposing potential for mechano-based therapeutic interventions,<sup>41</sup> although integrin-mediated contraction alteration of cardiomyocytes after carfilzomib treatment has not yet been

**Table 5. Top Downregulated DEPs in Cell Lysate**

Protein ID	Protein symbol	Description of full name	P value	Log <sub>2</sub> (fold change)
P28161	GSTM2	Glutathione S-transferase mu 2	0.000199	-0.37869
Q5XKP0	QIL1 (MICOS13)	Mitochondrial contact site and cristae organizing system subunit 13	0.000256	-0.38072
P14618	PKM	Pyruvate kinase M1/2	0.000615	-0.3854
O15067	PFAS	Phosphoribosylformylglycinamide synthase	0.001144	-0.39249
Q14254	FLOT2	Flotillin 2	0.001165	-0.39616
Q9HOR4	HDHD2	Haloacid dehalogenase like hydrolase domain containing 2)	0.00178	-0.39726
P29218	IMPA1	Inositol monophosphatase 1	0.002187	-0.39969
P30041	PRDX6	Peroxiredoxin 6	0.002598	-0.40337
P08243	ASNS	Asparagine synthetase (glutamine-hydrolyzing)	0.003198	-0.40509
P60174	TPI1	Triosephosphate isomerase 1	0.003513	-0.40568
Q3MHD2	LSM12	LSM12 homolog	0.004002	-0.40938
P48509	CD151	CD151 molecule (Raph blood group)	0.004477	-0.4101
P15259	PGAM2	Phosphoglycerate mutase 2	0.005065	-0.41576
Q16836	HADH	Hydroxyacyl-CoA dehydrogenase	0.005345	-0.41756
Q99541	PLIN2	(Perilipin 2)	0.006138	-0.42144
Q9Y235	APOBEC2	Apolipoprotein B mRNA editing enzyme catalytic subunit 2	0.006633	-0.42492
Q13813-2	SPTAN1	Spectrin alpha, non-erythrocytic 1	0.006885	-0.43392
O60669	SLC16A7	Solute carrier family 16 member 7	0.008852	-0.43623
Q96AX9	MIB2	Mindbomb E3 ubiquitin protein ligase 2	0.009051	-0.44424
P51553	IDH3G	Isocitrate dehydrogenase (NAD (+) 3 non-catalytic subunit gamma)	0.009335	-0.44433
P08133	ANXA6	Annexin A6	0.009685	-0.46695
P17174	GOT1	Glutamic-oxaloacetic transaminase 1	0.011001	-0.47138
P10109	FDX1	(Ferredoxin 1)	0.014375	-0.47543
P43007	SLC1A4	Solute carrier family 1 member 4	0.014845	-0.48642
P30046	DDT	D-dopachrome tautomerase	0.017058	-0.50283
Q13315	ATM	ATM serine/threonine kinase	0.0171	-0.50678
P34949	MPI	Mannose phosphate isomerase	0.018324	-0.50884
Q8IYM0	FAM186B	Family with sequence similarity 186 member B	0.018496	-0.51545
Q9NX18	SDHAF2	Succinate dehydrogenase complex assembly factor 2	0.021519	-0.51609
P80723	BASP1	Brain abundant membrane attached signal protein 1	0.022129	-0.52675
O75223	GGCT	Gamma-glutamylcyclotransferase)	0.022945	-0.53503
P17612	PRKACA	Protein kinase cAMP-activated catalytic subunit alpha	0.02751	-0.55372
P00374	DHFR	Dihydrofolate reductas	0.027565	-0.5787
Q8N111	CEND1	Cell cycle exits and neuronal differentiation 1	0.033353	-0.61374
B7Z596	TPM1	Tropomyosin 1	0.033428	-0.72819

DEPs indicates differentially expressed proteins.

characterized. This is the first study that applies a piconewton tension sensor to examine cytotoxic effects of carfilzomib on hiPSC-CMs. Using the TGT probes, we found that carfilzomib decreased integrin-mediated traction forces of hiPSC-CMs as measured by changes in fluorescence intensity on the probes because of contraction of individual cells. Our study provides a new avenue of mechano-pharmacology platform to study the impact of carfilzomib at molecular and cellular levels.

Recent evidence illustrates off-target effects of carfilzomib treatment in animal models; however,

mechanisms underlying contraction alteration after carfilzomib treatment in cardiomyocytes have not been fully characterized. Our findings indicate the possibility of on-target and off-target effects of carfilzomib on human cardiac cells. Using RNA-seq, we identified early transcriptomic signatures of carfilzomib-induced cardiotoxicity and important genes/pathways that might mediate carfilzomib-induced cell death and contraction defects. Following a 24-hour treatment of hiPSC-CMs with carfilzomib, there was significant upregulation of genes and related proteins involved

**Table 6. Top Upregulated DEPs in Cell Lysate**

Protein ID	Protein symbol	Description of full name	P value	Log <sub>2</sub> fold change
P17066	HSPA6	Heat shock protein family A (Hsp70) member 6	5.85E-06	2.920214
Q8N6M9	ZFAND2A	Zinc finger AN1-type containing 2A	8.86E-06	2.792291
P18847	ATF3	Activating transcription factor 3	2.03E-05	2.655011
Q15327	ANKRD1	Ankyrin repeat domain 1	2.93E-05	2.301373
O76080	ZFAND5	Zinc finger AN1-type containing 5	5.43E-05	2.210395
P08107	HSPA1A	Heat shock protein family A (Hsp70) member 1A	6.26E-05	2.166783
P38936	CDKN1A	Cyclin dependent kinase inhibitor 1	7.03E-05	2.135166
Q9H0R8	GABARAPL1	GABA type A receptor associated protein like 1	8.41E-05	1.985212
P25685	DNAJB1	DnaJ heat shock protein family (Hsp40) member B1	0.000163	1.945932
P04035	HMGCR	3-hydroxy-3-methylglutaryl-CoA reductase	0.000211	1.855423
P61587	RND3	Rho family GTPase 3	0.000249	1.649824
Q01581	HMGCS1	3-hydroxy-3-methylglutaryl-CoA synthase 1	0.000271	1.626212
O15525	MAFG	MAF bZIP transcription factor G	0.000284	1.601714
Q9H3F6	KCTD10	Potassium channel tetramerization domain containing 10	0.00037	1.507235
Q9UDY4	DNAJB4	DnaJ heat shock protein family (Hsp40) member B4	0.000379	1.484945
P54868	HMGCS2	3-hydroxy-3-methylglutaryl-CoA synthase 2	0.000395	1.463084
P02792	FTL	Ferritin light chain	0.000444	1.432189
Q9UBU8	MORF4L1	Mortality factor 4 like 1	0.000498	1.42401
Q9BYN0	SRXN1	Sulfiredoxin 1	0.000514	1.416937
Q92963	RIT1	Ras like without CAAX 1	0.000551	1.341017
P02511	CRYAB	(Crystallin alpha B)	0.000627	1.330892
Q9UH92	MLX	MAX dimerization protein MLX)	0.000713	1.30305
Q92598	HSPH1	(Heat shock protein family H (Hsp110) member 1)	0.00072	1.288595
Q99608	NDN	Necdin, MAGE family member	0.000767	1.265368
Q9BY42	RTFDC1	Replication termination factor 2	0.000826	1.221335
Q13501	SQSTM1	Sequestosome 1	0.000845	1.207748
P78362	SRPK2	SRSF protein kinase 2	0.000887	1.198661
Q9Y5A7	NUB1	Negative regulator of ubiquitin like proteins 1	0.000906	1.194131
P68133	ACTA1	Actin alpha 1, skeletal muscle	0.000913	1.178388
O60333-3	KIF1B	Kinesin family member 1B	0.000962	1.153891
P62699	YPEL5	Yippee like 5	0.001058	1.125207
O75794	CDC123	Cell division cycle 12	0.001082	1.097219
O95817	BAG3	BAG cochaperone 3	0.001229	1.091382
O43164	PJA2	Praja ring finger ubiquitin ligase 2	0.001327	1.058091
Q07352	ZFP36L1	ZFP36 ring finger protein like 1	0.00139	1.046927
O14950	MYL12B	Myosin light chain 12B	0.001602	1.007005
Q9UGL1	KDM5B	Lysine demethylase 5B	0.001648	0.977882
P24844	MYL9	Myosin light chain 9	0.001717	0.966276
Q9UK73	FEM1B	Fem-1 homolog B	0.00174	0.953693
Q8TEY7	USP33	Ubiquitin specific peptidase 33	0.001752	0.948084
P0CG47	UBB	Ubiquitin B	0.001801	0.928962
P46976	GYG1	Glycogenin 1	0.001869	0.926016

DEPs indicates differentially expressed proteins.

in cellular stress. In particular, RNA-seq revealed that carfilzomib treatment induced the overexpression of genes encoding HSPs including *HSPA1B*, *HSPA1A*, and *HSPA6*. Consistent with our RNA-seq data, the

proteomic analysis also confirmed upregulation of HSPs in both the cell lysate and the secretome, including HSPAB1, and HSPA1A as well as molecules that act as cochaperones including DNAJA&B, HSPH1,

**Table 7. Top Dysregulated DEPs in Secretome**

Protein ID	Protein symbol	Description of full name	P value	Log <sub>2</sub> fold change
P01009	SERPINA1	Serpin family A member 1	0.002177	-1.01851
P09871	C1S	Complement C1s	0.005218	-0.71786
Q9UBP4	DKK3	Dickkop WNT signaling pathway inhibitor 3	0.00526	0.74339
P08107	HSPA1A	Heat shock protein family A (Hsp70) member 1A	0.005936	1.115906
Q15063	POSTN	Periostin	0.006501	-0.55999
O60814	HIST1H2BK	H2B clustered	0.006567	-0.27213
P55083	MFAP4	Microfibril associated protein 4	0.007602	-0.69158
Q86UP2	KTN1	Kinectin 1	0.011208	0.152319
Q12841	FSTL1	Follistatin like 1	0.012976	-0.5254
P08238	HSP90AB1	Heat shock protein 90 alpha family class B member 1	0.013136	-0.13566
P02461	COL3A1	Collagen type III alpha 1 chain	0.013179	-0.55331
P26038	MSN	Moesin	0.013885	0.42732
O95373	IPO7	Importin 7	0.014671	-0.63705
P11142	HSPA8	Heat shock protein family A (Hsp70) member 8	0.016105	0.364134
P31946	YWHA8	Tyrosine 3-monooxygenase/tryptophan 5-monooxygenase activation protein beta)	0.016696	0.35428
P08123	COL1A2	Collagen type I alpha 2 chain	0.017711	-0.45736
Q14315	FLNC	Filamin C	0.021456	0.693258
P02751	FN1	Fibronectin 1	0.021493	-0.54779
P13929	ENO3	Enolase 3	0.024012	-0.33332
Q7Z7M1	GPR144	ADGRD2- adhesion G protein-coupled receptor D2	0.024362	3.30262
P55072	VCP	Valosin containing protein	0.025906	0.830314
P05121	SERPINE1	Serpin family E member 1	0.027676	0.433167
P26038	MSN	Moesin	0.013885	0.42732
P50502	ST13	ST13 Hsp70 interacting protein	0.044477	0.412665

DEPs indicates differentially expressed proteins.

ZFAND2A, and CRYAB. It has been reported that proteasome inhibitors such as bortezomib can upregulate HSPs,<sup>42</sup> and targeting HSPs has been considered to

overcome resistance to chemotherapeutic agents such as imatinib and cisplatin.<sup>43</sup> HSP90 has been found to assist in degrading toxic metabolites by promoting

**Table 8. Downregulated DEPs in Secretome and Their Association With KEGG Pathways**

Gene ID	Protein symbol	Description of full name	P value	Log <sub>2</sub> fold change	KEGG pathway
ENSG00000177943	MAMDC4	MAM domain containing 4	4.94E-56	-9.19909	None
ENSG00000171992	SYNPO	Synaptopodin	8.84E-51	-6.60094	N/A
ENSG00000104738	MCM4	Minichromosome maintenance complex component 4	1.11E-50	-6.26153	(ko04530) Tight junction; (hsa04530) Tight junction
ENSG00000137809	ITGA11	Integrin subunit alpha 11	2.58E-48	-6.19687	(ko03030) DNA replication; (hsa03030) DNA replication; (ko04110) Cell cycle
ENSG00000184347	SLIT3	Slit guidance ligand 3	5.13E-46	-6.15778	(ko05412) Arrhythmogenic right ventricular cardiomyopathy (ARVC); (hsa05412) Arrhythmogenic right ventricular cardiomyopathy; (ko04512) ECM-receptor interaction
ENSG00000156427	FGF18	Fibroblast growth factor 18	6.14E-43	-6.15087	(ko04360) Axon guidance; (hsa04360) Axon guidance
ENSG00000185567	AHNAK2	AHNAK nucleoprotein 2	3.69E-39	-6.08355	(ko05218) Melanoma; (hsa05218) Melanoma; (ko05224) Breast cancer
ENSG00000128951	DUT	Deoxyuridine triphosphatase	7.18E-39	-6.01202	N/A
ENSG00000225138	SLC9A3-AS1	None	1.01E-38	-5.97976	(ko00240) Pyrimidine metabolism; (hsa00240) Pyrimidine metabolism; (hsan01) drug metabolism

DEPs indicates differentially expressed proteins; and KEGG, *Kyoto Encyclopedia of Genes and Genomes*.



**Table 9. GO Terms and KEGG Pathways Associated With Overlapped Genes/Proteins Identified by DEPs From Cell Lysate and DEGs by RNA-seq**

Description	Category	Count	GO/KEGG term ID	Adjusted P value	Enrichment
Response to heat	GO term biological processes	15	GO:0009408	1E-15	40
Heat shock protein binding	GO term molecular functions	10	GO:0031072	7.9E-10	35
ATPase regulator activity	GO term molecular functions	6	GO:0060590	5E-07	65
ATPase activator activity	GO term molecular functions	4	GO:0001671	0.00016	71
Ferroptosis	KEGG pathway	4	ko04216	0.00079	44
Necroptosis	KEGG pathway	6	hsa04217	0.00079	16
Tau protein binding	GO term molecular functions	4	GO:0048156	0.001	39
Myeloid cell activation involved in immune response	GO term biological processes	9	GO:0002275	0.00126	7.3
Chaperone-mediated autophagy	GO term biological processes	3	GO:0061684	0.00158	83
Positive regulation of ATPase activity	GO term biological processes	4	GO:0032781	0.002	32
Apoptotic signaling pathway	GO term biological processes	9	GO:0097190	0.00251	6.5
ATPase activity	GO term molecular functions	7	GO:0016887	0.00501	8.3
Regulation of ATPase activity	GO term biological processes	4	GO:0043462	0.00631	22
Cellular response to interleukin 1	GO term biological processes	5	GO:0071347	0.01	12
Interleukin 1-mediated signaling pathway	GO term biological processes	4	GO:0070498	0.01259	17
Stress-activated MAPK cascade	GO term biological processes	5	GO:0051403	0.05012	7.7
Regulation of extrinsic apoptotic signaling pathway	GO term biological processes	4	GO:2001236	0.05012	11
Intrinsic apoptotic signaling pathway	GO term biological processes	5	GO:0097193	0.05012	7.7
Regulation of intrinsic apoptotic signaling	GO term biological processes	4	GO:2001242	0.0631	11
Response to oxidative stress	GO Biological Processes	6	GO:0006979	0.0631	5.8
Extrinsic apoptotic signaling pathway via death domain receptors	GO term biological processes	3	GO:0008625	0.1	15
Regulation of reactive oxygen species metabolic process	GO term biological processes	4	GO:2000377	0.1	8.9
Autophagy	GO term biological processes	6	GO:0006914	0.11749	4.9
Positive regulation of cell death	GO term biological processes	7	GO:0010942	0.12589	4.2
Pathways in cancer	KEGG pathway	6	hsa05200	0.15136	4.6
Mitogen-activated protein kinase (MAPK) signaling pathway	KEGG pathway	4	ko04010	0.19953	7
Apoptotic mitochondrial changes	GO term biological processes	3	GO:0008637	0.2138	11
ATPase activity, coupled	GO term molecular functions	4	GO:0042623	0.2138	6.8
Macro autophagy	GO term biological processes	4	GO:0016236	0.35481	5.6
Cellular senescence	KEGG pathway	3	hsa04218	0.42658	7.7
Oxidoreductase activity	GO molecular functions	6	GO:0016491	0.43652	3.5
PI3K-Akt signaling pathway	KEGG pathway	4	ko04151	0.4466	5.2
Regulation of Ras protein signal transduction	GO term biological processes	3	GO:0046578	0.56234	6.8
Regulation of MAPK cascade	GO term biological processes	5	GO:0043408	0.025119	2.9
Wnt signaling pathway	GO term biological processes	4	GO:0016055	0.031623	3.4
Cell-cell signaling by wnt	GO term biological processes	4	GO:0198738	0.031623	3.4
Retina-expressed kinase (ERK)1 and ERK2 cascade	GO term biological processes	3	GO:0070371	0.039811	4
Regulation of mitogen-activated protein kinase activity	GO term biological processes	3	GO:0043405	0.039811	3.8

DEGs indicates differentially expressed genes; DEPs, differentially expressed proteins; GO, gene ontology; KEGG, *Kyoto Encyclopedia of Genes and Genomes*; and RNA-seq, RNA sequencing.

ubiquitination and proteasome lysis.<sup>44</sup> Overexpression of HSPs is also linked to many pathological conditions,<sup>45,46</sup> and increased HSPs have a protective function by blocking apoptosis, which allows cells to survive in otherwise lethal conditions.<sup>47,48</sup> It is likely that increased HSPs may overcome the toxic effect of the inhibition of proteasomes after carfilzomib treatment in hiPSC-CMs. Given that increased HSPs are detectable in the secretome following the carfilzomib treatment, these HSPs may serve as biomarkers for early detection of carfilzomib-induced cardiotoxicity.

Our results highlight the possible role of the ECM and integrins in contractility defects as an early response to carfilzomib treatment. Alterations in ECM can impact cardiomyocyte function.<sup>49,50</sup> ECM and secreted proteins are important components of the stroma, which could play important roles in the cell-cell communication and regulation of cell process including contraction.<sup>51</sup> Integrins are sensors that transmit mechanical signals to ion channels.<sup>52</sup> The results of the GO term analysis indicate that genes belong to the ECM, integrin complex, and actinin cytoskeleton proteins were downregulated in carfilzomib-treated cells. Carfilzomib treatment also downregulated genes associated with cardiac muscle cell contraction, including contractile proteins (eg, MYL2 and MYH6) and Ca<sup>2+</sup> handling proteins. In line with RNA-seq data, our proteome data in both cell lysate and secretome also indicate significant reduction of proteins related to both contraction and ECM including POSTN, COL3A1, THBS1, C1S, ANXA6, and TPM.

The current results demonstrate that carfilzomib interferes with mitochondrial function as indicated by reduced ATP production and respiration, increased mitochondrial ROS, and decreased mitochondrial membrane potentials. The reduced mitochondrial function and cellular energy impairment may contribute to cardiomyocyte dysfunction, which is consistent with previously published in vivo off-target effects of carfilzomib.<sup>53</sup> Increased mitochondrial ROS is known to be associated with cytotoxicity.<sup>35,38,54</sup> We also found similar results of increased mitochondrial ROS by treating hiPSC-CMs with doxorubicin, a cancer therapy drug with well-known cardiovascular toxicity effect because of the generation of ROS,<sup>55,56</sup> reduced contractile capacity,<sup>57</sup> and adverse effect on Ca<sup>2+</sup> transport.<sup>31</sup> The increased mitochondrial ROS and decreased mitochondrial function in carfilzomib-treated hiPSC-CMs were also associated with the downregulation of genes associated with mitochondrial function such as nicotinamide adenine dinucleotide (NADH) ubiquinone oxidoreductase subunit AB1, which is a crucial regulator of mitochondrial energy and ROS metabolism through coordinating the assembly of respiratory complexes.<sup>58</sup> In addition, our proteomic analysis indicated downregulation of SDHFA2, a member of succinate

dehydrogenase complex, which plays essential roles in both the mitochondrial electron transport chain and the tricarboxylic acid cycle.

Consistent with the findings on increased mitochondrial oxidative stress, defects in mitochondrial function, and increased gene expression and proteins related to response to oxidative stress in carfilzomib-treated hiPSC-CMs, we found that cell death in carfilzomib-treated hiPSC-CMs could be rescued by targeting oxidative stress with ascorbic acid. These results suggest that oxidative stress plays an important role in carfilzomib-induced cytotoxicity and that antioxidants have the potential for cardioprotective therapy.

The carfilzomib-induced mitochondrial changes may lead to other functional alterations including abnormal Ca<sup>2+</sup> signaling. On the other hand, abnormal Ca<sup>2+</sup> signaling can induce alterations in respiratory chain complexes, which lead to increased mitochondrial oxidative stress and reduced mitochondrial membrane potential.<sup>35,37</sup> Our results showed a significant increase in Ca<sup>2+</sup> transient abnormalities after carfilzomib treatment, which is consistent with clinical observations showing arrhythmias after chemotherapeutic drugs as a common phenomenon.<sup>40,59</sup> In pathological conditions, Ca<sup>2+</sup> overload is accompanied by alterations in mitochondrial function and mitochondrial membrane potential,<sup>37,38,60</sup> and abnormal Ca<sup>2+</sup> transients can be an indicator for proarrhythmic behavior of cardiomyocytes.<sup>61</sup> In cardiomyocytes, the interplay between Ca<sup>2+</sup> signaling and mitochondrial function is necessary to maintain normal cardiac function.<sup>22,37</sup> Carfilzomib treatment of hiPSC-CMs significantly downregulated several genes encoding Ca<sup>2+</sup> handling proteins, including *RYR2* and *CASQ2*, which play a critical role in excitation–contraction coupling in cardiomyocytes. Consistently, carfilzomib treatment increased abnormal Ca<sup>2+</sup> transients in hiPSC-CMs. Our findings support that possible mechanisms of carfilzomib-induced cardiotoxicity are associated with abnormal Ca<sup>2+</sup> signaling and mitochondrial oxidative stress, contributing to the development of arrhythmias after carfilzomib treatment.

We also found that carfilzomib treatment reduced the expression of proteins associated with metabolic process. For example, carfilzomib reduced the expression of glucose metabolism-related enzymes including PKM2 and PRKACA. Loss of function studies show that *PKM2* deletion in cardiomyocytes resulted in significantly reduced cell cycle.<sup>62</sup> PRKACA is a key regulatory enzyme in humans and contributes to the control of cellular processes including glucose metabolism and cell division. Defective regulation of protein kinase A activity is also linked to the progression of cardiovascular disease, and reduced protein kinase A activity is associated with reduction of Ca<sup>2+</sup> signaling in embryonic hearts.<sup>63</sup> In addition, carfilzomib dysregulated the

expression of proteins involved in autophagy, apoptosis, and cell cycle. For example, carfilzomib downregulated CLEC16A, a regulator of autophagy through mTOR (the mammalian target of rapamycin) activity,<sup>64</sup> and upregulated ATG101 (an autophagy factor required for autophagosome formation), CDKN1A (a regulator of cell cycle in response to stress stimuli), and RND3 (a member of the small Rho GTPase family that regulates apoptosis through the Rho kinase-dependent signaling pathway).

Considering the complexity of cardiotoxicity, several possible mechanisms can synergistically induce cytotoxic effects after carfilzomib treatment. As expected from its on-target effect, proteasome inhibition by carfilzomib treatment can promote cell death. Our study also reveals potential novel mechanisms induced by carfilzomib-treatment, including (1) targeting mitochondria that may lead to oxidative stress, disruptions in cellular energy, and contractility defect; and (2) triggering downregulation of ECM and integrin-related genes that may result in reduced integrin-mediated traction forces and alterations of cell structure and morphology.

We note that a replication study in human patients is an important next step to examine if the alterations of genes and proteins observed in hiPSC-CMs are also observed in human patients. However, given the similar end points observed in hiPSC-CMs and human patients (eg, cytotoxicity and abnormal contractility), the findings of hiPSC-CMs from this study may have important implications toward discovery of new therapies to overcome clinical side effects after chemotherapeutic drug treatment. In addition, molecular changes, such as upregulation of heat shock-related genes and other proteins, may provide a new avenue toward biomarker development for early detection of carfilzomib-induced cardiotoxicity.

## ARTICLE INFORMATION

Received April 27, 2021; accepted October 1, 2021.

### Affiliations

Division of Pediatric Cardiology, Department of Pediatrics, Emory University School of Medicine and Children's Healthcare of Atlanta, Atlanta, GA (P.F., R.L., D.L., M.R.L., H.H., J.T.M., C.X.); Biomolecular Chemistry, Department of Chemistry, Emory University, Atlanta, GA (A.R., K.S.); School of Chemistry and Biochemistry and the Petit Institute for Bioengineering and Bioscience, Georgia Institute of Technology, Atlanta, GA (F.S., R.W.); Department of Medicine & Winship Cancer Institute, Emory University School of Medicine, Atlanta, GA (A.M.); and Wallace H. Coulter Department of Biomedical Engineering, Georgia Institute of Technology and Emory University, Atlanta, GA (K.S., C.X.).

### Acknowledgments

Drs Forghani, Mandawat, and Xu conceived and designed research. Dr Forghani, A. Rashid, Dr Sun, M. R. Lee, and Dr Li performed research and acquired the data. Dr Forghani, A. Rashid, Dr Sun, R. Liu, M.R. Lee, Dr Li, H. Hwang, and Dr Maxwell analyzed and interpreted the data. Dr Forghani, Dr Sun, and R. Liu performed statistical analysis. Dr Mandawat provided clinical guidance. Drs Wu and Salaita contributed new reagents or analytic tools, interpreted the data, and made critical revision of the article for important

intellectual content. Drs Forghani and Xu wrote the article and made critical revisions of the article for important intellectual content. Dr Xu handled funding and supervision.

### Sources of Funding

This study was supported by the Children's Heart Research and Outcomes Center at Emory University and Children's Healthcare of Atlanta; the Center for Pediatric Technology and Biocology at Emory University and Georgia Institute of Technology; Imagine, Innovate and Impact (I3) Funds from the Emory School of Medicine and through the Georgia Clinical and Translational Science Awards Program (the National Institutes of Health award) (UL1-TR002378); the National Institutes of Health (R21AA025723, R01HL136345, and R01AA028527); and the National Science Foundation and the Center for the Advancement of Science in Space (CBET 1926387).

### Disclosures

None.

## REFERENCES

- Cole DC, Frishman WH. Cardiovascular complications of proteasome inhibitors used in multiple myeloma. *Cardiol Rev*. 2018;26:122–129. doi: 10.1097/CRD.0000000000000183
- Kuhn DJ, Chen Q, Voorhees PM, Strader JS, Shenk KD, Sun CM, Demo SD, Bennett MK, van Leeuwen FWB, Chanan-Khan AA, et al. Potent activity of carfilzomib, a novel, irreversible inhibitor of the ubiquitin-proteasome pathway, against preclinical models of multiple myeloma. *Blood*. 2007;110:3281–3290. doi: 10.1182/blood-2007-01-065888
- Dimopoulos MA, Roussou M, Gavriatopoulou M, Psimenou E, Ziogas D, Eleutherakis-Papaikovou E, Fotiou D, Migkou M, Kanellias N, Panagiotidis I, et al. Cardiac and renal complications of carfilzomib in patients with multiple myeloma. *Blood Adv*. 2017;1:449–454. doi: 10.1182/bloodadvances.2016003269
- Mangla A, Paydary K, Liu J, Mbachi C, Yim B, Lad TE. Carfilzomib-associated cardiovascular adverse events in a non-caucasian cohort of patients with multiple myeloma: a real-world experience. *Hematol Oncol*. 2018;36:715–717. doi: 10.1002/hon.2535
- Moreau P, Richardson PG, Cavo M, Orlowski RZ, San Miguel JF, Palumbo A, Harousseau JL. Proteasome inhibitors in multiple myeloma: 10 years later. *Blood*. 2012;120:947–959. doi: 10.1182/blood-2012-04-403733
- Jain T, Narayanasamy H, Mikhael J, Reeder CB, Bergsagel PL, Mayo A, Stewart AK, Mookadam F, Fonseca R. Systolic dysfunction associated with carfilzomib use in patients with multiple myeloma. *Blood Cancer J*. 2017;7:642. doi: 10.1038/s41408-017-0026-7
- Bruno G, Bringham S, Maffei I, Iannaccone A, Crea T, Ravera A, Astarita A, Vallelonga F, Salvini M, Gay F, et al. Cardiovascular organ damage and blood pressure levels predict adverse events in multiple myeloma patients undergoing carfilzomib therapy. *Cancers (Basel)*. 2019;11:622. doi: 10.3390/cancers11050622
- Shah C, Bishnoi R, Jain A, Bejjanki H, Xiong S, Wang Y, Zou F, Moreb JS. Cardiotoxicity associated with carfilzomib: systematic review and meta-analysis. *Leuk Lymphoma*. 2018;59:2557–2569. doi: 10.1080/10428194.2018.1437269
- Waxman AJ, Clasen S, Hwang W-T, Garfall A, Vogl DT, Carver J, O'Quinn R, Cohen AD, Stadtmauer EA, Ky B, et al. Carfilzomib-associated cardiovascular adverse events: a systematic review and meta-analysis. *JAMA Oncol*. 2018;4:e174519. doi: 10.1001/jamaoncol.2017.4519
- Kortuem KM, Stewart AK. Carfilzomib. *Blood*. 2013;121:893–897. doi: 10.1182/blood-2012-10-459883
- Hahn VS, Zhang KW, Sun L, Narayan V, Lenihan DJ, Ky B. Heart failure with targeted cancer therapies: mechanisms and cardioprotection. *Circ Res*. 2021;128:1576–1593. doi: 10.1161/CIRCRESAHA.121.318223
- Han B, Yao W, Oh YT, Tong JS, Li S, Deng J, Yue P, Khuri FR, Sun SY. The novel proteasome inhibitor carfilzomib activates and enhances extrinsic apoptosis involving stabilization of death receptor 5. *Oncotarget*. 2015;6:17532–17542. doi: 10.18632/oncotarget.3947
- Hasinoff BB, Patel D, Wu X. Molecular mechanisms of the cardiotoxicity of the proteasomal-targeted drugs bortezomib and carfilzomib. *Cardiovasc Toxicol*. 2017;17:237–250. doi: 10.1007/s12012-016-9378-7
- Efentakis P, Kremastiotis G, Varela A, Nikolaou P-E, Papanagnou E-D, Davos CH, Tsoumani M, Agrogiannis G, Konstantinidou A, Kastiris

- E, et al. Molecular mechanisms of carfilzomib-induced cardiotoxicity in mice and the emerging cardioprotective role of metformin. *Blood*. 2019;133:710–723. doi: 10.1182/blood-2018-06-858415
15. Musunuru K, Sheikh F, Gupta RM, Houser SR, Maher KO, Milan DJ, Terzic A, Wu JC; American Heart Association Council on Functional G, Translational B. Induced pluripotent stem cells for cardiovascular disease modeling and precision medicine: a scientific statement from the American Heart Association. *Circ Genom Precis Med*. 2018;11:e000043. doi: 10.1161/HCG.0000000000000043
  16. Mordwinkin NM, Burrige PW, Wu JC. A review of human pluripotent stem cell-derived cardiomyocytes for high-throughput drug discovery, cardiotoxicity screening, and publication standards. *J Cardiovasc Transl Res*. 2013;6:22–30. doi: 10.1007/s12265-012-9423-2
  17. Hnatiuk AP, Briganti F, Staudt DW, Mercola M. Human iPSC modeling of heart disease for drug development. *Cell Chem Biol*. 2021;28:271–282. doi: 10.1016/j.chembiol.2021.02.016
  18. Bellin M, Mummery CL. Inherited heart disease—what can we expect from the second decade of human iPSC cell research? *FEBS Lett*. 2016;590:2482–2493.
  19. Mercola M, Colas A, Willems E. Induced pluripotent stem cells in cardiovascular drug discovery. *Circ Res*. 2013;112:534–548. doi: 10.1161/CIRCRESAHA.111.250266
  20. Nair P, Prado M, Perea-Gil I, Karakikes I. Concise review: precision matchmaking: induced pluripotent stem cells meet cardio-oncology. *Stem Cells Transl Med*. 2019;8:758–767. doi: 10.1002/sctm.18-0279
  21. Singh P, Wang X, Hageman L, Chen Y, Magdy T, Landier W, Ginsberg JP, Neglia JP, Sklar CA, Castellino SM, et al. Association of GSTM1 null variant with anthracycline-related cardiomyopathy after childhood cancer—a Children's Oncology Group ALTE03N1 report. *Cancer*. 2020;126:4051–4058. doi: 10.1002/cncr.32948
  22. Lan F, Lee A, Liang P, Sanchez-Freire V, Nguyen P, Wang LI, Han L, Yen M, Wang Y, Sun N, et al. Abnormal calcium handling properties underlie familial hypertrophic cardiomyopathy pathology in patient-specific induced pluripotent stem cells. *Cell Stem Cell*. 2013;12:101–113. doi: 10.1016/j.stem.2012.10.010
  23. Jha R, Wu Q, Singh M, Preininger MK, Han P, Ding G, Cho HC, Jo H, Maher KO, Wagner MB, et al. Simulated microgravity and 3D culture enhance induction, viability, proliferation and differentiation of cardiac progenitors from human pluripotent stem cells. *Sci Rep*. 2016;6:30956. doi: 10.1038/srep30956
  24. Billis P, Will Y, Nadanaciva S. High-content imaging assays for identifying compounds that generate superoxide and impair mitochondrial membrane potential in adherent eukaryotic cells. *Curr Protoc Toxicol*. 2014;59:25.1.1–25.1.14. doi: 10.1002/0471140856.tx2501s59
  25. Rampoldi A, Crooke SN, Preininger MK, Jha R, Maxwell J, Ding L, Spearman P, Finn MG, Xu C. Targeted elimination of tumorigenic human pluripotent stem cells using suicide-inducing virus-like particles. *ACS Chem Biol*. 2018;13:2329–2338. doi: 10.1021/acscchembio.8b00490
  26. Huebsch N, Loskill P, Mandegar MA, Marks NC, Sheehan AS, Ma Z, Mathur A, Nguyen TN, Yoo JC, Judge LM, et al. Automated video-based analysis of contractility and calcium flux in human-induced pluripotent stem cell-derived cardiomyocytes cultured over different spatial scales. *Tissue Eng Part C Methods*. 2015;21:467–479. doi: 10.1089/ten.tec.2014.0283
  27. Gao W, Shi P, Chen X, Zhang L, Liu J, Fan X, Luo X. Clathrin-mediated integrin alphaIIb beta3 trafficking controls platelet spreading. *Platelets*. 2018;29:610–621.
  28. Liu Y, Blanchfield L, Ma VP, Andargachew R, Galior K, Liu Z, Evavold B, Salaita K. DNA-based nanoparticle tension sensors reveal that T-cell receptors transmit defined pN forces to their antigens for enhanced fidelity. *Proc Natl Acad Sci USA*. 2016;113:5610–5615. doi: 10.1073/pnas.1600163113
  29. Ma R, Kellner AV, Ma VP, Su H, Deal BR, Brockman JM, Salaita K. DNA probes that store mechanical information reveal transient piconewton forces applied by T cells. *Proc Natl Acad Sci USA*. 2019;116:16949–16954. doi: 10.1073/pnas.1904034116
  30. Liu R, Sun F, Forghani P, Armand LC, Rampoldi A, Li D, Wu R, Xu C. Proteomic profiling reveals roles of stress response, Ca(2+) transient dysregulation, and novel signaling pathways in alcohol-induced cardiotoxicity. *Alcohol Clin Exp Res*. 2020;44:2187–2199.
  31. Hanna AD, Lam A, Tham S, Dulhunty AF, Beard NA. Adverse effects of doxorubicin and its metabolic product on cardiac RyR2 and SERCA2A. *Mol Pharmacol*. 2014;86:438–449. doi: 10.1124/mol.114.093849
  32. Takemura G, Fujiwara H. Doxorubicin-induced cardiomyopathy from the cardiotoxic mechanisms to management. *Prog Cardiovasc Dis*. 2007;49:330–352. doi: 10.1016/j.pcad.2006.10.002
  33. Maillet A, Tan K, Chai X, Sadananda SN, Mehta A, Ooi J, Hayden MR, Pouladi MA, Ghosh S, Shim W, et al. Modeling doxorubicin-induced cardiotoxicity in human pluripotent stem cell derived-cardiomyocytes. *Sci Rep*. 2016;6:25333. doi: 10.1038/srep25333
  34. Polonchuk L, Chabria M, Badi L, Hoflack JC, Figtree G, Davies MJ, Gentile C. Cardiac spheroids as promising in vitro models to study the human heart microenvironment. *Sci Rep*. 2017;7:7005. doi: 10.1038/s41598-017-06385-8
  35. Starkov AA. The role of mitochondria in reactive oxygen species metabolism and signaling. *Ann N Y Acad Sci*. 2008;1147:37–52. doi: 10.1196/annals.1427.015
  36. Bernardi P, Di Lisa F, Fogolari F, Lippe G. From ATP to PTP and back: a dual function for the mitochondrial ATP synthase. *Circ Res*. 2015;116:1850–1862. doi: 10.1161/CIRCRESAHA.115.306557
  37. Brookes PS, Yoon Y, Robotham JL, Anders MW, Sheu SS. Calcium, ATP, and ROS: a mitochondrial love-hate triangle. *Am J Physiol Cell Physiol*. 2004;287:C817–C833. doi: 10.1152/ajpcell.00139.2004
  38. Indo HP, Davidson M, Yen HC, Suenaga S, Tomita K, Nishii T, Higuchi M, Koga Y, Ozawa T, Majima HJ. Evidence of ROS generation by mitochondria in cells with impaired electron transport chain and mitochondrial DNA damage. *Mitochondrion*. 2007;7:106–118. doi: 10.1016/j.mito.2006.11.026
  39. Sabharwal SS, Schumacker PT. Mitochondrial ROS in cancer: initiators, amplifiers or an Achilles' heel? *Nat Rev Cancer*. 2014;14:709–721. doi: 10.1038/nrc3803
  40. Buza V, Rajagopalan B, Curtis AB. Cancer treatment-induced arrhythmias: focus on chemotherapy and targeted therapies. *Circ Arrhythm Electrophysiol*. 2017;10:e005443. doi: 10.1161/CIRCEP.117.005443
  41. Lampi MC, Reinhart-King CA. Targeting extracellular matrix stiffness to attenuate disease: from molecular mechanisms to clinical trials. *Sci Transl Med*. 2018;10:eaao0475. doi: 10.1126/scitranslmed.aao0475
  42. Shah SP, Nooka AK, Jaye DL, Bahlis NJ, Lonial S, Boise LH. Bortezomib-induced heat shock response protects multiple myeloma cells and is activated by heat shock factor 1 serine 326 phosphorylation. *Oncotarget*. 2016;7:59727–59741. doi: 10.18632/oncotarget.10847
  43. Lu XY, Xiao L, Wang L, Ruden DM. Hsp90 inhibitors and drug resistance in cancer: the potential benefits of combination therapies of Hsp90 inhibitors and other anti-cancer drugs. *Biochem Pharmacol*. 2012;83:995–1004. doi: 10.1016/j.bcp.2011.11.011
  44. Pratt WB, Morishima Y, Peng HM, Osawa Y. Proposal for a role of the Hsp90/Hsp70-based chaperone machinery in making triage decisions when proteins undergo oxidative and toxic damage. *Exp Biol Med (Maywood)*. 2010;235:278–289. doi: 10.1258/ebm.2009.009250
  45. Kamal A, Boehm MF, Burrows FJ. Therapeutic and diagnostic implications of Hsp90 activation. *Trends Mol Med*. 2004;10:283–290. doi: 10.1016/j.molmed.2004.04.006
  46. Hoter A, El-Sabban ME, Naim HY. The HSP90 family: structure, regulation, function, and implications in health and disease. *Int J Mol Sci*. 2018;19:2560. doi: 10.3390/ijms19092560
  47. Creagh EM, Sheehan D, Cotter TG. Heat shock proteins—modulators of apoptosis in tumour cells. *Leukemia*. 2000;14:1161–1173. doi: 10.1038/sj.leu.2401841
  48. Lanneau D, Brunet M, Frisan E, Solary E, Fontenay M, Garrido C. Heat shock proteins: essential proteins for apoptosis regulation. *J Cell Mol Med*. 2008;12:743–761. doi: 10.1111/j.1582-4934.2008.00273.x
  49. Boothe SD, Myers JD, Pok S, Sun J, Xi Y, Nieto RM, Cheng J, Jacot JG. The effect of substrate stiffness on cardiomyocyte action potentials. *Cell Biochem Biophys*. 2016;74:527–535.
  50. Tallawi M, Rai R, Boccaccini AR, Aifantis KE. Effect of substrate mechanics on cardiomyocyte maturation and growth. *Tissue Eng Part B Rev*. 2015;21:157–165. doi: 10.1089/ten.teb.2014.0383
  51. Schelbert EB, Fonarow GC, Bonow RO, Butler J, Gheorghiade M. Therapeutic targets in heart failure: refocusing on the myocardial interstitium. *J Am Coll Cardiol*. 2014;63:2188–2198. doi: 10.1016/j.jacc.2014.01.068
  52. Becchetti A, Petroni G, Arcangeli A. Ion channel conformations regulate integrin-dependent signaling. *Trends Cell Biol*. 2019;29:298–307. doi: 10.1016/j.tcb.2018.12.005
  53. Moreb JS. Off-target effects of carfilzomib that cause cardiotoxicity. *Blood*. 2019;133:626–628. doi: 10.1182/blood-2018-12-889758



54. Raturi A, Simmen T. Where the endoplasmic reticulum and the mitochondrion tie the knot: the mitochondria-associated membrane (MAM). *Biochim Biophys Acta*. 2013;1833:213–224. doi: 10.1016/j.bbamcr.2012.04.013
55. Arai M, Yoguchi A, Takizawa T, Yokoyama T, Kanda T, Kurabayashi M, Nagai R. Mechanism of doxorubicin-induced inhibition of sarcoplasmic reticulum Ca(2+)-ATPase gene transcription. *Circ Res*. 2000;86:8–14.
56. Berthiaume JM, Wallace KB. Adriamycin-induced oxidative mitochondrial cardiotoxicity. *Cell Biol Toxicol*. 2007;23:15–25. doi: 10.1007/s10565-006-0140-y
57. Dimitrakis P, Romay-Ogando MI, Timolati F, Suter TM, Zuppinger C. Effects of doxorubicin cancer therapy on autophagy and the ubiquitin-proteasome system in long-term cultured adult rat cardiomyocytes. *Cell Tissue Res*. 2012;350:361–372. doi: 10.1007/s00441-012-1475-8
58. Hou T, Zhang R, Jian C, Ding W, Wang Y, Ling S, Ma Q, Hu X, Cheng H, Wang X. NDUFB1 confers cardio-protection by enhancing mitochondrial bioenergetics through coordination of respiratory complex and supercomplex assembly. *Cell Res*. 2019;29:754–766. doi: 10.1038/s41422-019-0208-x
59. Guglin M, Aljayeh M, Saiyad S, Ali R, Curtis AB. Introducing a new entity: chemotherapy-induced arrhythmia. *Europace*. 2009;11:1579–1586. doi: 10.1093/europace/eup300
60. Sauer H, Wartenberg M, Hescheler J. Reactive oxygen species as intracellular messengers during cell growth and differentiation. *Cell Physiol Biochem*. 2001;11:173–186. doi: 10.1159/000047804
61. Filice D, Dhahri W, Solan JL, Lampe PD, Steele E, Milani N, Van Biber B, Zhu W-Z, Valdman TS, Romagnuolo R, et al. Optical mapping of human embryonic stem cell-derived cardiomyocyte graft electrical activity in injured hearts. *Stem Cell Res Ther*. 2020;11:417. doi: 10.1186/s13287-020-01919-w
62. Magadum A, Singh N, Kurian AA, Munir I, Mehmood T, Brown K, Sharkar MTK, Chepurko E, Sassi Y, Oh JG, et al. Pkm2 regulates cardiomyocyte cell cycle and promotes cardiac regeneration. *Circulation*. 2020;141:1249–1265. doi: 10.1161/CIRCULATIONAHA.119.043067
63. Sui X, Kong N, Ye L, Han W, Zhou J, Zhang Q, He C, Pan H. p38 and JNK MAPK pathways control the balance of apoptosis and autophagy in response to chemotherapeutic agents. *Cancer Lett*. 2014;344:174–179. doi: 10.1016/j.canlet.2013.11.019
64. Tam RC, Li MW, Gao YP, Pang YT, Yan S, Ge W, Lau CS, Chan VS. Human CLEC16A regulates autophagy through modulating mTOR activity. *Exp Cell Res*. 2017;352:304–312. doi: 10.1016/j.yexcr.2017.02.017